

A Sequential flow process of CO₂ capture and conversion using cost-effective porous organic polymers

Zhongqi Wu^{1#}, Zhong Li^{1#}, Lei Hu¹, Samson Afewerki², Maria Strømme², Qian-Feng Zhang¹, Chao Xu^{*1,2}

¹*Institute of Molecular Engineering and Applied Chemistry, Anhui University of Technology, Ma'anshan, 243002 (P. R. China)*

²*Division of Nanotechnology and Functional Materials, Department of Materials Science and Engineering, Ångström Laboratory, Uppsala University, 75121 Uppsala (Sweden)*

#These authors contributed equally to this work

E-mail: chao.xu@angstrom.uu.se

Experimental section

Materials

2,6-diaminopyridine (2,6-DAP) was purchased from Alfa Aesar, 3,5-diaminopyridine (3,5-DAP), 4,4-biphenyldicarboxaldehyde (BDA) were purchased from Tensus Biotech, terephthalaldehyde (TPA), isophthalaldehyde (IPA), 2-phenylethylamine, 4-methoxybenzylamine, propargylic bromide, sodium bicarbonate, anhydrous sodium carbonate, 1,8-Diazabicyclo[5.4.0]undec-7-ene (DBU), were purchased from McLean Chemical Reagent, methanol, ethanol, acetone, ether, THF, DMF, acetonitrile, dichloromethane, petroleum ether, ethyl acetate, acetic acid, were purchased from Sinopharm-Group, *N*-methylpropargylamine was purchased from Leyan Reagent, aniline, benzylamine, were purchased from Rhawn Reagent, tert-butylthiol (t-BuSH) and triethylamine were purchased from Aladdin Scientific, silver trifluoroacetate (CF₃COOAg) was purchased from Bide Pharm, and silver nitrate (AgNO₃) was purchased from Sinopharm-Group. All of the chemicals were used without further purification.

Synthesis

Synthesis of 3,5-DAP-TPA POP

TPA (0.5 mmol, 67 mg) was mixed with 2.5 mL of ethanol in an autoclave, followed by adding 2 mL aqueous acetic acid solution (9 M). The mixture was stirred at room temperature for 20 min. Separately, 3,5-DAP (54.5 mg, 0.5 mmol) was dissolved in 2.5 mL of ethanol and the solution was added into the TPA solution. The mixture was stirred at room temperature for additional 30 min. Subsequently, the mixture was sealed in a stainless-steel autoclave and then heated in an oven at 120 °C for 72 h. After the end of the reaction, it was filtered through qualitative filter paper. The obtained solid was thoroughly washed by water, ethanol and acetone and extracted with ethanol for 12 h then dried at 70 °C for 24 h. The final product was a brownish yellow powder with a yield of 98%.

Table S1 A summary of synthesis, yield and BET surface area of 3,5-DAP-TPA POP under different synthesis conditions

Entry	Solvent	Time (hour)	C _(Monomer) (M)	Temperature (°C)	C _(AcOH) (M)	BET surface area (m ² /g)	Yield (%)
1	EtOH	72	0.1	60	3	149	60
2	EtOH	72	0.1	60	9	276	65
3	EtOH	72	0.1	120	3	482	96
4	EtOH	72	0.1	120	9	540	98
5	EtOH	72	0.2	120	9	489	99
6	EtOH	24	0.2	120	9	379	96
7	EtOH	72	0.4	120	9	449	99

Note: Volume of EtOH is 5 mL and volume of aqueous acetic acid solution is 2 mL.

Synthesis of 3,5-DAP-IPA POP

The synthesis followed the procedures for synthesizing conditions for 3,5-DAP-TPA and IPA (0.5 mmol, 67 mg) was used instead of TPA. A brownish yellow powder was obtained in 98% yield.

Synthesis of 3,5-DAP-BDA POP

BDA (1 mmol, 210 mg) was mixed with 2.5 mL of ethanol in an autoclave, followed by adding 2 mL aqueous acetic acid solution (17.5 M). The mixture was stirred at room temperature for 20 min. Separately, 3,5-DAP (109 mg, 1 mmol) was dissolved in 2.5 mL of ethanol and the solution was added into the TPA solution. The mixture was stirred at room temperature for additional 30 min. Subsequently, the mixture was sealed in a stainless-steel autoclave and then heated in an oven at 120 °C for 72 h. After the end of the reaction, it was filtered through qualitative filter paper. The obtained solid was thoroughly washed by water, ethanol and acetone and extracted with ethanol for 12 h then dried at 70 °C for 24 h. The final product was a brownish yellow powder with a yield of 93%.

Table S2 A summary of synthesis, yield and BET surface area of 3,5-DAP-BDA POP under different synthesis conditions

Entry	Solvent	Time (hour)	C _(Monomer) (M)	Temperature (°C)	C _(AcOH) (M)	BET surface area (m ² /g)	Yield (%)
1	EtOH	72	0.1	120	9	16	73
2	EtOH	72	0.2	120	9	322	91
3	EtOH	72	0.2	120	17.5	512	93

Note: Volume of EtOH is 5 mL and volume of aqueous acetic acid solution is 2 mL.

Synthesis of 2,6-DAP-TPA POP

TPA (2 mmol, 268 mg) was mixed with 2.5 mL of ethanol in an autoclave, followed by adding 2 mL aqueous acetic acid solution (9 M). The mixture was stirred at room temperature for 20 min. Separately, 2,6-DAP (2 mmol, 218 mg) was dissolved in 2.5 mL of ethanol and the solution was added into the TPA solution. The mixture was stirred at room temperature for additional 30 min. Subsequently, the mixture was sealed in a stainless-steel autoclave and then heated in an oven at the 120 °C for 24 h. After the end of the reaction, it was filtered through qualitative filter paper. The obtained solid was thoroughly washed by water, ethanol and acetone and extracted with ethanol for 12 h then dried at 70 °C for 24 h. The final product was a brownish yellow powder with a yield of ~100%.

Table S3 A summary of synthesis, yield and BET surface area of 2,6-DAP-TPA POP under different synthesis conditions

Entry	Solvent	Time (hour)	C _(Monomer) (M)	Temperature (°C)	C _(AcOH) (M)	S _{BET} (m ² /g)	Yield (%)
1	EtOH	72	0.2	25	3	10	60
2	EtOH	72	0.1	25	9	–	12
3	EtOH	72	0.2	25	9	23	25
4	EtOH	24	0.2	60	9	118	55
5	EtOH	24	0.2	80	9	314	55
6	EtOH	24	0.4	80	9	333	77
7	EtOH	72	0.2	80	9	422	99
8	EtOH	72	0.4	80	9	454	99
9	EtOH	72	0.1	120	9	332	97
10	EtOH	72	0.2	120	9	419	>99
11	EtOH	72	0.4	120	9	572	>99
12	EtOH	24	0.2	120	9	584	>99
13	EtOH	24	0.4	120	9	587	>99

Note: Volume of EtOH is 5 mL and volume of aqueous acetic acid solution is 2 mL.

Synthesis of 2,6-DAP-IPA POP

The synthesis was followed the procedures for synthesizing conditions for 2,6-DAP-TPA and IPA (0.2 mmol, 268 mg) was used instead of TPA. A brownish yellow powder was obtained in ~100% yield.

Synthesis of 2,6- DAP-BDA POP

The synthesis was followed the procedures for synthesizing conditions for 2,6-DAP-TPA and BDA (2 mmol, 420 mg) was used instead of TPA. A brownish yellow powder was obtained in 99% yield.

Large scale synthesis of 2,6-DAP-TPA POP

TPA (100 mmol, 13.4 g) was mixed with 250 mL of ethanol in 1 L polypropylene plastic drum, followed by adding 2 mL aqueous acetic acid solution (9 M). The mixture was stirred at room temperature for 20 min. Separately, 2,6-DAP (100 mmol, 10.9 g) was dissolved in 250 mL of ethanol and the solution was added into the TPA solution. The mixture was stirred at room temperature for additional 30 min. Subsequently, the mixture was heated in an oven at 80 °C for 3 days. After the end of the reaction, it was filtered through qualitative filter paper. The obtained solid was thoroughly washed by water, ethanol and acetone and extracted with ethanol for 12 h then dried at 70 °C for 24 h. The final product was a brownish yellow powder with a yield of 98%. The product was named LSS-2,6-DAP-TPA POP. (LSS: large scale synthesis).

Table S4 A summary of synthesis, yield, and BET surface area of LSS-2,6-DAP-TPA POP at a large scale under different synthesis conditions.

Entry	Solvent (mL)	Time (hour)	C _(Monomer) (M)	Temperature (°C)	V _(AcOH) (mL)	S _{BET} (m ² /g)	Yield (%)
1	EtOH (500)	72	0.1	60	200	339	31
2	EtOH (50)	72	0.2	80	20	458	93
3	EtOH (250)	72	0.2	80	100	486	93
4	EtOH (500)	72	0.2	80	200	745	98

Note: the concentration of aqueous acetic acid solution is 9 M

Table S5 Cost calculation for large scale synthesis of 2,6-DAP-TPA POP

	Chemical	Price (USD/kg)	Amount (kg)	Cost (USD)
Lab-scale synthesis	2,6-diaminopyridine ^a	93.84	0.545	51.14
	Terephthalaldehyde ^b	22.08	0.67	14.79
	Ethanol ^c	0.66	12.5	0.825 ^d
	Glacial acetic acid ^e	4.02	10	4.02 ^d
	2,6-DAP-TPA POP	64.34^f	1.1^f	70.78

	Chemical ^g	Price (USD/ton)	Amount (ton)	Cost (USD)
Industrial-scale synthesis	2,6-diaminopyridine	1104	0.545	601.7
	terephthalaldehyde	1311	0.67	878.4
	Ethanol ^c	593	12.5	741.2 ^d
	Glacial acetic acid	442	10	442 ^d
	2,6-DAP-TPA POP	2421.2	1.1^f	2663.3

^a Wuhan Lullaby Pharmaceutical Chemical, 99% purity; ^b Jiangsu Aikon, 98% purity; ^c 99% purity, prices are found via <http://www.zhengxingxincailiao.com/>.

^d In industrial production, the solvent and catalyst can be recycled. It is assumed that 10% of the solvent and catalyst are lost during each batch reaction. Therefore, this 10% loss is accounted for in the cost estimation of the required solvent and catalyst.

^e Sinopharm-Group, 99.5% purity.

^f based on 98% yield.

^g Industrial grade; prices are found via <https://www.100ppi.com/> and <https://china.guidechem.com/>

Note: The calculation is based only on the cost of chemicals, providing a preliminary estimation of the synthesis cost. However, the actual production cost would be much higher since it doesn't include other expenses such as equipment depreciation, transport, labor, energy, and waste treatment.

Synthesis of Ag₃₃ ^[1]

(^tBuSAg)_n ^[2] (19.7 mg, 0.1 mmol) was added to a mixed solvent (1 mL of CH₃CN/1 mL of MeOH). The mixture was subjected to ultrasonication for 5 min and a homogeneous suspension was formed. Subsequently, a solution of CF₃COOAg (44.0 mg, 0.2 mmol) in 0.5 mL of CH₃CN and 0.5 mL of MeOH was then added to this suspension, resulting in the immediate formation of a clear yellow solution. This solution was ultrasonicated for an additional 10 min. Slow evaporation of the solution in dark yielded the product as yellow crystals. Yield: 72.3%.

Synthesis of Ag₃₃-POP

In a 50 mL round-bottom flask, 100 mg of grounded POP powder (3,5-DAP-TPA POP, 3,5-DAP-IPA POP, 3,5-DAP-BDA POP, 2,6-DAP-TPA POP, 2,6-DAP-IPA POP, 2,6-DAP-BDA POP) were mixed with 8 mL of a methanol solution containing 50 mg of Ag₃₃. The mixture was stirred at 35 °C for 12 h. The resulting solid was then thoroughly washed with methanol, and acetone, and dried at 50 °C overnight. The final product was a brownish-yellow powder. The respective Ag₃₃-POP variants (Ag₃₃-3,5-DAP-TPA POP, Ag₃₃-3,5-DAP-IPA POP, Ag₃₃-3,5-DAP-BDA POP, Ag₃₃-2,6-DAP-TPA POP, Ag₃₃-2,6-DAP-IPA POP, Ag₃₃-2,6-DAP-BDA POP) were obtained. The Ag contents, determined by ICP-OES, were 2.47 wt%, 1.05 wt%, 1.41 wt%, 1.76 wt%, 2.75 wt%, and 1.52 wt%, respectively.

Characterizations

Infrared spectra were recorded using a Nicolet-6700 spectrometer. The samples were ground with potassium bromide and pressed into transparent pellets for measurement. Solid-state ^{13}C nuclear magnetic resonance (NMR) spectra of the POPs were recorded on a Bruker AVWBIII600 spectrometer. Approximately 200 mg of the POP powder sample was used for the solid-state NMR measurement. Liquid ^1H NMR spectra were recorded using a Bruker Avance 400 MHz spectrometer. Powder X-ray diffraction (XRD) patterns were recorded on a Rigaku Ultima IV diffractometer. X-ray photoelectron spectra (XPS) were recorded on a Thermo Scientific K-Alpha X-ray Photoelectron Spectrometer. Scanning electron microscopy (SEM) and transmission electron microscopy (TEM) images were recorded using a Zeiss Leo Gemini 1530 SEM instrument and a JEOL JEM-2100 TEM instrument, respectively. Thermogravimetric analysis (TGA) curves were recorded on a Mettler Toledo TGA/SDTA851e thermogravimetric analyzer under a N_2 or air atmosphere (flow rate: 60 mL/min) at temperatures ranging from 25 to 800 °C with a heating rate of 5 °C/min.

Gas sorption isotherms were recorded using a Micromeritics ASAP 2020 surface area and porosity analyser. Before the measurements, the samples were degassed at 150 °C for 12 h under a kinetic vacuum ($<10^{-5}$ mmHg). N_2 sorption isotherms were recorded at 77 K to analyze the porosity of the samples and the surface area was calculated from the N_2 adsorption isotherms using Brunauer–Emmett–Teller (BET) theory. Pore size distribution was analyzed using the adsorption isotherm based on the density functional theory model. CO_2 and N_2 sorption isotherms were recorded at 273, 293, and 298 K at the pressure range of 0–1 bar. In addition, a Kubo-X1000 surface area and porosity analyser was used to measure N_2 sorption isotherms of the POPs at 77 K for screening studies.

CO_2 -over- N_2 selectivity was calculated from single component adsorption isotherm using deal Adsorbed Solution Theory (IAST).^[3] A gas mixture component of 15v% CO_2 /85v% N_2 was used for the calculation. For the calculations, the measured CO_2 and N_2 adsorption isotherms were fitted by dual-site and single-site Langmuir equations respectively.

Dual-site Langmuir equation:

$$q = q_{sat, A} * b_A * p / (1 + b_A * p) + q_{sat, B} * b_B * p / (1 + b_B * p),$$

Single-site Langmuir equation:

$$q = q_{sat} * b * p / (1 + b * p)$$

where q is adsorption capacity (mmol/g), q_{sat} is saturation adsorption capacity (mmol/g), p is pressure (Pa), and b is Langmuir constant (Pa), A and B are distinct adsorption sites.

Breakthrough measurements

The breakthrough measurements were recorded using a breakthrough analyser (CT-41, Xuzhou Beifang Gaorui Electronic Equipment Co., Ltd) coupled with a gas chromatography analyzer (GC-9860, Nanjing Hope Analytical Equipment Co., Ltd.) equipped with a thermal conductivity detector (TCD). The measurements were carried out at a pressure of 1 bar and a set temperature. A stainless-steel column with a length of 20 cm and an internal diameter of 0.6 cm ($V_{\text{column}} = 0.30 \text{ cm} \times 0.30 \text{ cm} \times 3.14 \times 20.00 \text{ cm} = 5.652 \text{ cm}^3$) was packed with 1.0 g POPs sample. Different gas mixtures were used as the stock gas for separation. The gas mixture, consisting of CO_2 and N_2 at specific concentrations, was prepared by mixing pure CO_2 and N_2 gases. The concentration of each gas in the mixture was controlled by regulating the flow rate of each component using mass flow controllers (MFCs). To introduce moisture into the CO_2/N_2 gas mixture, a third gas line with 100% relative humidity (RH) N_2 , generated by bubbling pure N_2 through water, was added to the CO_2 and N_2 mixture. The flow rate of this humidified N_2 was also regulated by a MFC to achieve the desired RH in the final gas mixture. To evaluate the performance of the POPs for practical CO_2 capture from flue gas, a pilot-scale breakthrough experiment

was conducted. The experiment utilized a stainless-steel column with a length of 20 cm and an internal diameter of 1.9 cm ($V_{\text{column}} = 0.95 \text{ cm} \times 0.95 \text{ cm} \times 3.14 \times 20.00 \text{ cm} = 56.677 \text{ cm}^3$), packed with 15 g of POP.

The gas mixture was passed through the POP column at a desired flow rate of 2–10 mL/min. The eluted gas at the outlet was analyzed using the GC analyzer, with the analysis performed every 1.2 minutes. Breakthrough curves were plotted based on the GC results.

Continuous CO₂ capture from simulated flue gas

The CO₂ capture system consists of two stainless steel columns, each filled with 15 g of LSS-2,6-DAP-TPA POP, interconnected with three-way valves (Fig. 3k). The ends of the columns are connected to a 250 mL round-bottom flask, which collects the separated gas and is equipped with a pressure gauge to monitor pressure changes during gas collection. A gas mixture containing 15v%/85v% CO₂/N₂, simulating flue gas, is introduced into the columns at flow rates of either 2 or 10 mL/min for the CO₂ capture process.

The operational procedure is as follows: Initially, the entire system is vacuumed. Following this, the simulated flue gas is directed through POP bed 1, controlled by a MFC. This column adsorbs CO₂ until it reaches saturation. During the adsorption process, the end of the column is connected to the atmosphere to allow the eluted N₂ to be released. Upon the saturation of POP bed 1, which is determined by breakthrough measurements at a given flow rate, Valve 1 is switched to direct the flue gas flow through POP bed 2. Simultaneously, the saturated POP bed 1 is connected to a round-bottom flask and the column is heated to 150 °C with a heating jacket. This heating facilitates the release of the adsorbed gas, which is then collected in the flask. The captured gas can either be compressed and stored or directly converted into fine chemicals. Once POP bed 1 has cooled and regenerated, it is ready for reuse in the flue gas separation process. Simultaneously, the saturated POP bed 2 is heated so that the adsorbed gas can be eluted and collected. By alternating between the two beds and repeating these steps, the system achieves continuous CO₂ capture from simulated flue gas.

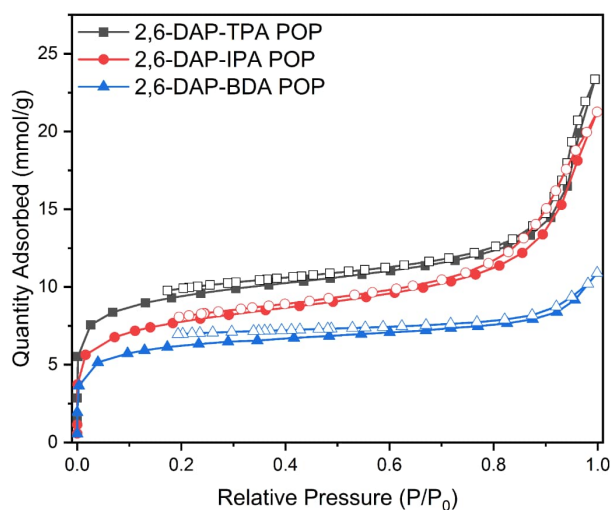


Fig. S1 N₂ sorption isotherms of 2,6-DAP-TPA POP, 2,6-DAP-BDA POP and 2,6-DAP-IPA POP recorded at 77 K.

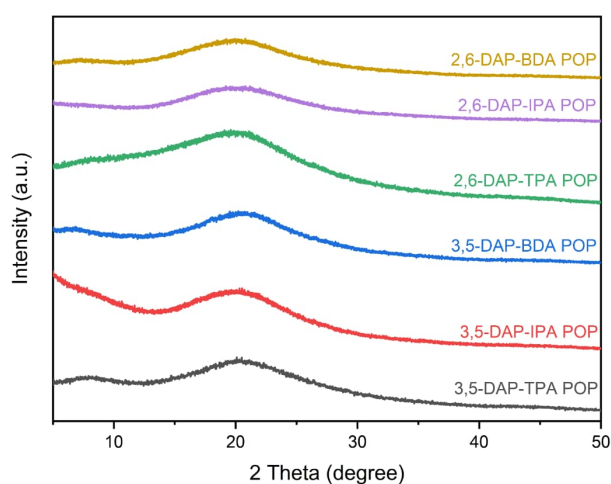


Fig. S2 Powder X-ray diffraction patterns of the POPs. The results indicate that the POPs are mainly amorphous.

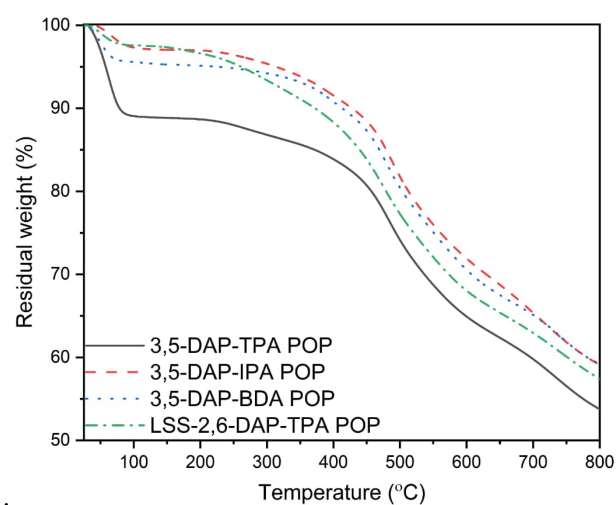
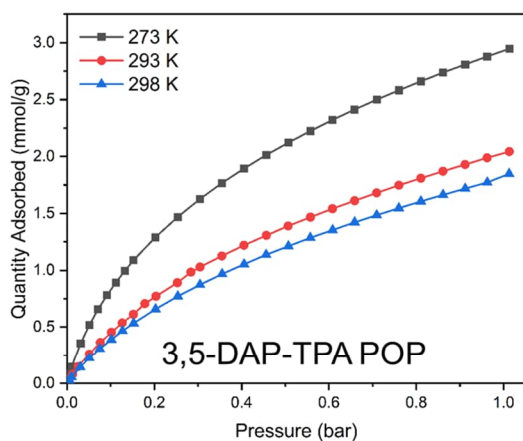
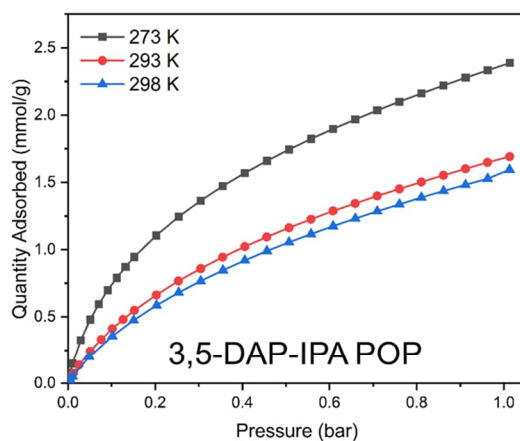


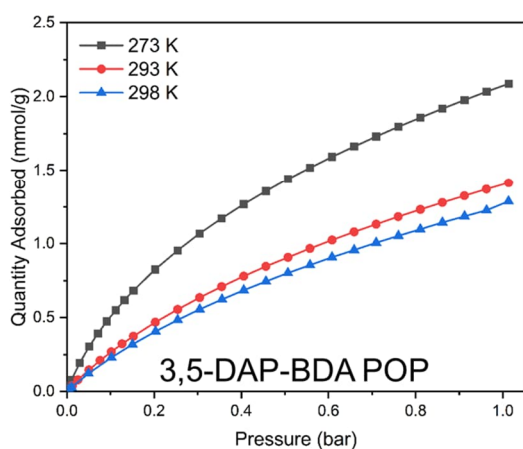
Fig. S3 Thermogravimetric curves of 3,5-DAP-TPA POP, 3,5-DAP-IPA POP, 3,5-DAP-BDA POP, LSS-2,6-DAP-TPA POP recorded under N₂ atmosphere. The results indicate that the POPs have high thermal stability with onset decomposition temperature of > 400 °C.



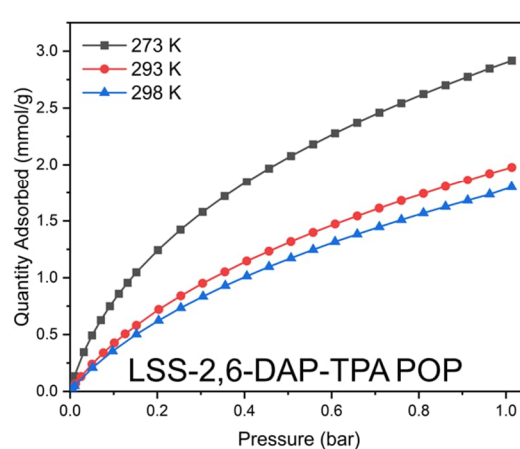
(a)



(b)



(c)



(d)

Fig. S4 CO₂ adsorption isotherms of 3,5-DAP-TPA POP, 3,5-DAP-IPA POP, 3,5-DAP-BDA POP, LSS-2,6-DAP-TPA POP at different temperatures (273, 293 and 298 K).

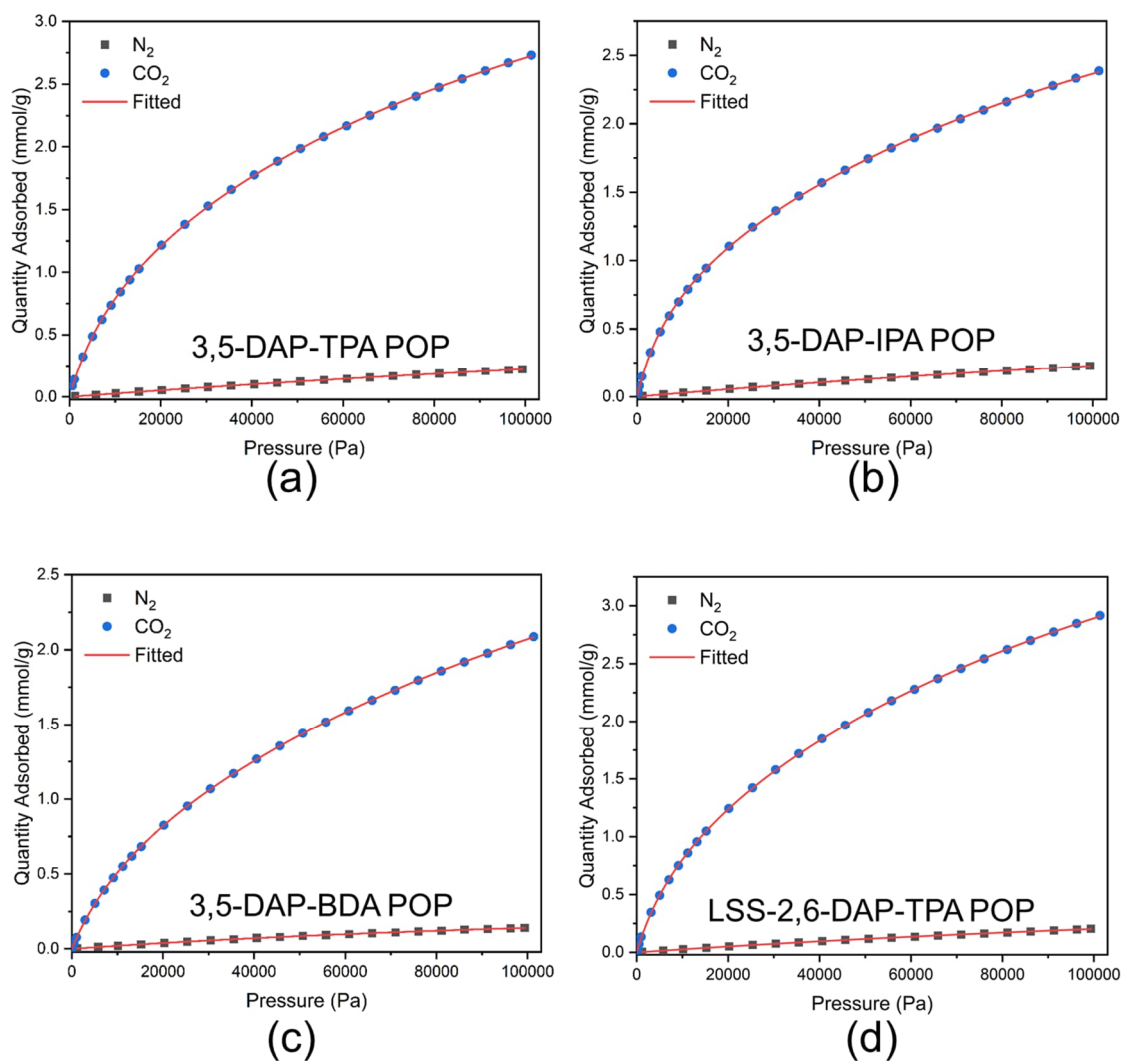


Fig. S5 CO₂ and N₂ adsorption isotherms of 3,5-DAP-TPA POP, 3,5-DAP-IPA POP, 3,5-DAP-BDA POP, LSS-2,6-DAP-TPA POP at 273 K. The red curves show the fitted results. CO₂ adsorption isotherms were fitted by dual-site Langmuir model, while N₂ adsorption isotherms were fitted by single site Langmuir model. The fitted results are presented in Table S6.

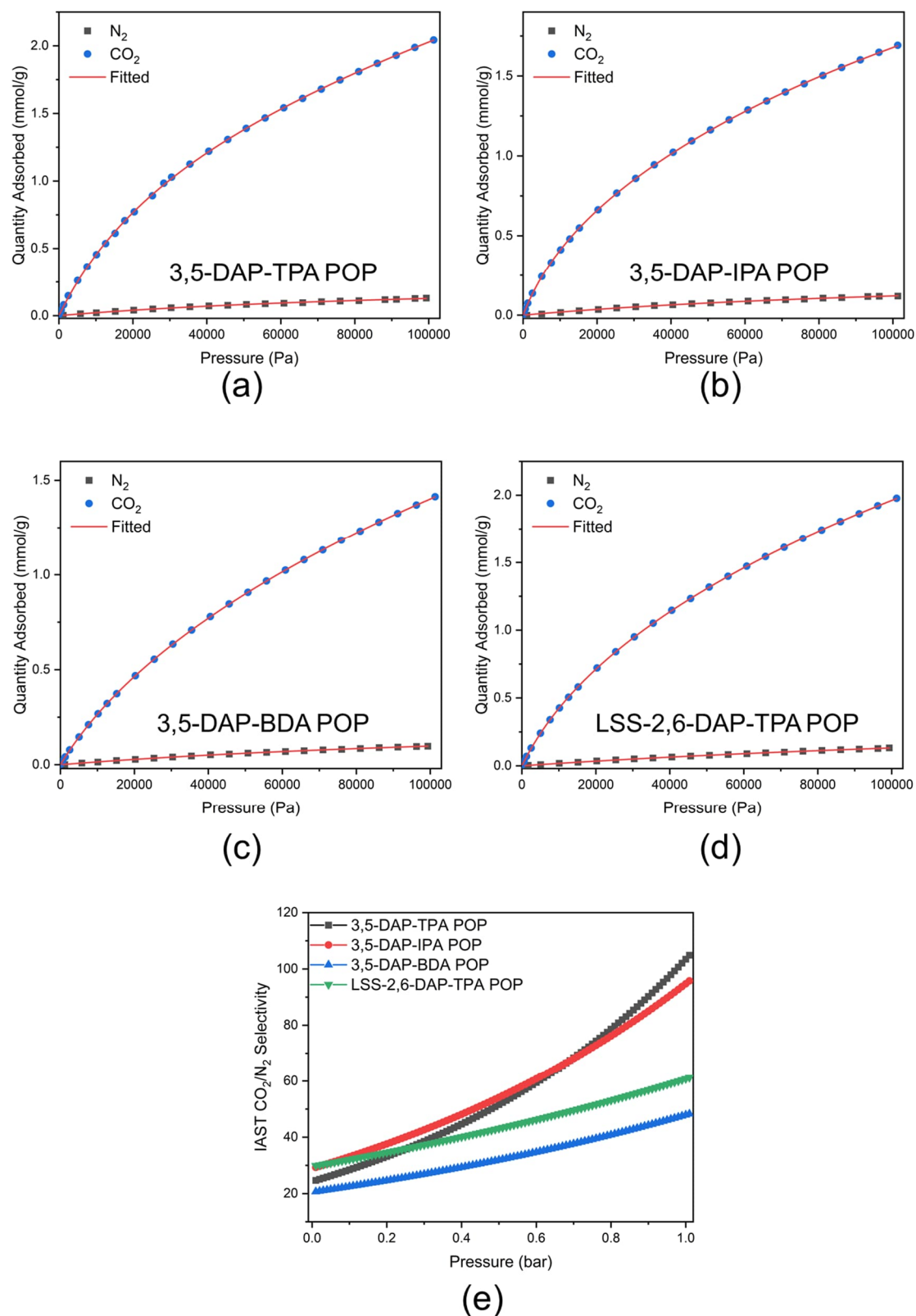


Fig. S6 CO₂ and N₂ adsorption isotherms of (a) 3,5-DAP-TPA POP, (b) 3,5-DAP-IPA POP, (c) 3,5-DAP-BDA POP, (d) LSS-2,6-DAP-TPA POP at 293 K, and (e) the CO₂-over-N₂ selectivities of the POPs at 293 K. The red curves represent the fitted results. The CO₂ adsorption isotherms were fitted using a dual-site Langmuir model, while the N₂ adsorption isotherms were fitted using a single-site Langmuir model. The fitted results are presented in Table S7.

Table S6 Fitted parameters for the CO₂ and N₂ adsorption data of POPs at 273 K

	Gas	Q _{sat, A} (mmol/g)	b _A (Pa ⁻¹)	Q _{sat, B} (mmol/g)	b _B (Pa ⁻¹)	Adj. R ²
3,5-DAP-TPA	CO ₂	0.99	1.07E-4	4.87	7.07E-6	0.99998
	N ₂	1.58	2.06E-6	-	-	0.99979
3,5-DAP-IPA	CO ₂	0.86	1.37E-4	3.85	6.84E-6	0.99995
	N ₂	1.08	2.66E-6	-	-	0.99972
3,5-DAP-BDA	CO ₂	0.72	7.27E-5	4.33	4.96E-6	0.99999
	N ₂	0.40	5.39E-6	-	-	0.99972
LSS-2,6-DAP-TPA	CO ₂	0.91	1.11E-4	5.06	2.04E-5	0.99998
	N ₂	0.80	3.41E-6	-	-	0.99949

Note: The adsorption data was recorded at 273 K and 0–1 bar. The CO₂ and N₂ adsorption data were fitted by dual-site Langmuir and single-site Langmuir model, respectively.

Table S7 Fitted parameters for the CO₂ and N₂ adsorption data of POPs at 293K

	Gas	Q _{sat, A} (mmol/g)	b _A (Pa ⁻¹)	Q _{sat, B} (mmol/g)	b _B (Pa ⁻¹)	Adj. R ²
3,5-DAP-TPA POP	CO ₂	1.50	3.10E-5	10.21	9.60E-7	0.99991
	N ₂	0.28	2.61E-6	-	-	0.99979
3,5-DAP-IPA POP	CO ₂	0.56	7.45E-5	3.55	5.01E-6	0.99998
	N ₂	0.29	7.16E-6	-	-	0.99841
3,5-DAP-BDA POP	CO ₂	0.46	3.95E-5	4.06	3.41E-6	0.99999
	N ₂	0.26	5.97E-6	-	-	0.99964
LSC-2,6-DAP-TPA POP	CO ₂	0.71	5.08E-5	4.86	3.91E-6	0.99999
	N ₂	0.45	4.15E-6	-	-	0.99971
Ag ₃₃ -3,5-DAP-TPA POP	CO ₂	0.59	6.31E-5	4.14	5.11E-6	0.99999
	N ₂	0.90	2.18E-6	-	-	0.99986

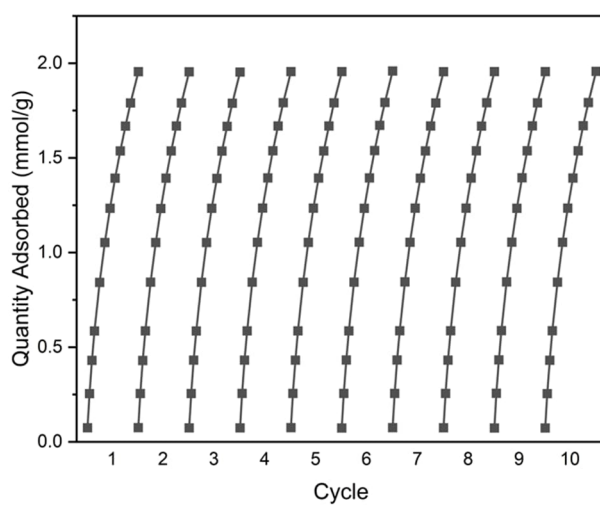
Note: The adsorption data was recorded at 293 K and 0–1 bar. The CO₂ and N₂ adsorption data were fitted by dual-site Langmuir and single-site Langmuir model, respectively

Table S8 A summary of CO₂ capture performance of different POPs

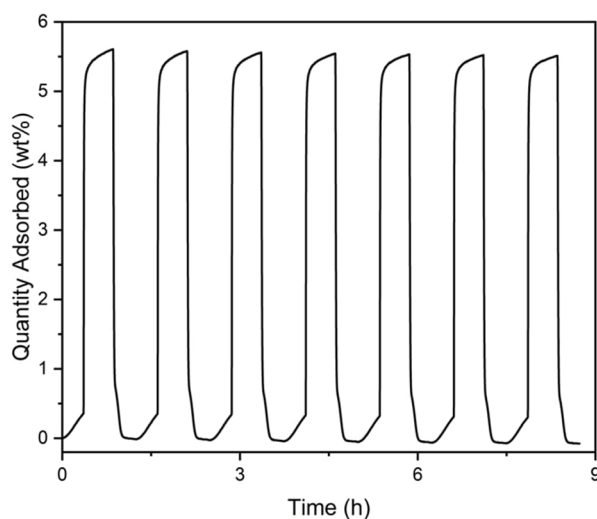
Sample	S _{BET} (m ² /g)	T (K)	CO ₂ uptake at 1 bar (mmol/g)	Q _{st} (kJ/mol)	CO ₂ /N ₂ selectivity	Ref.
3,5-DAP-TPA POP	540	273 K	2.95	—	48 ^a	This work
		293 K	2.04	29.4	105 ^a	
		298 K	1.85	—	—	
3,5-DAP-IPA POP	340	273 K	2.39	—	62 ^a	
		293 K	1.69	32.7	96 ^a	
		298 K	1.59	—	—	
3,5-DAP-BDA POP	512	273 K	2.09	—	94 ^a	
		293 K	1.41	29.4	48 ^a	
		298 K	1.89	—	—	
LSS-2,6-DAP-TPA POP	745	273 K	2.92	—	94 ^a	
		293 K	1.98	32.5	61 ^a	
		298 K	1.80			
POP-P	826	273 K	2.61	36.1	32.6 ^a	4
POP-O	920	273 K	2.52	28.3	23.4 ^a	
POP-M	1130	273 K	3.02	25.9	18.3 ^a	
PDVB-VP-0.1	603	273 K	2.19	—	104.4 ^a	5
PDVB-VP-0.25	489	273 K	2.37	—	140.7 ^a	
CTF-1	746	273 K	2.47	27.5	20 ^a	6
FCTF-1	662	273 K	4.67	35.0	31 ^a	
HCP-MAAMs	298	273 K	1.56	—	104 ^a	7
FC-POP	1540	273 K	3.1	26.4	12.62 ^a	8
HTM	5	273 K	1.68	29.9	71.7 ^a	9
HTM-MA	587	273 K	3.91	31.3	58.4 ^a	
sPI-1	1108	273 K	5.40	33	40 ^a	10
DCBP-CTF-1	2437	298 K	2.07	24.1	13 ^a	11
F-DCBP-CTF-1	1574	298 K	3.82	33.1	31 ^a	
CTF-3	1454	298 K	1.34	21	24.5 ^a	12
F12CTF-3	1558	298 K	4.33	24.5	32.4 ^a	
CXF1-OMe	626	273 K	1.49	26	—	13
CFX1-OH	540	273 K	2.20	35	98 ^a	

TNHCP1	848	298 K	2.20	30.8	30 ^a	
TNHCP2	766	298 K	2.11	32.8	42 ^a	14
TNHCP3	751	298 K	2.23	32.7	45 ^a	

Note: –, not available. ^a IAST model. ^b Henry law.



(a)



(b)

Fig. S7 (a) Cyclic adsorption isotherms of LSS-2,6-DAP-TPA under vacuum swing adsorption conditions, recorded at 293 K. The sample was regenerated by vacuum without additional heating between cycles. (b) Gravimetric CO₂ adsorption cycles for LSS-2,6-DAP-TPA were conducted under temperature swing adsorption conditions at 298 K, with a CO₂ flow rate of 60 mL/min. Before each cycle, the sample was reactivated at 150 °C in an N₂ atmosphere.

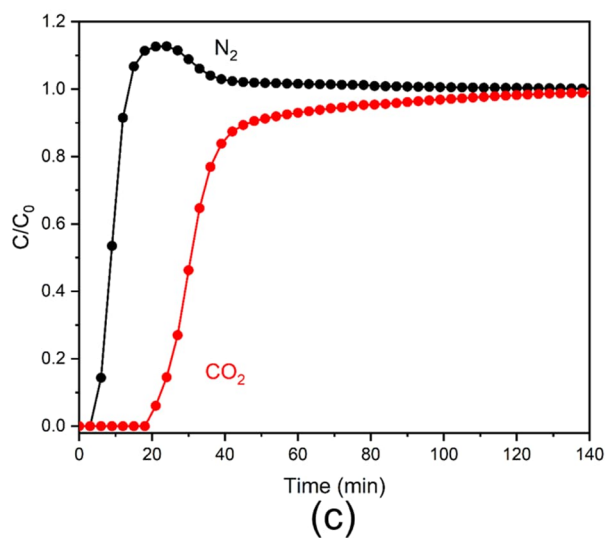
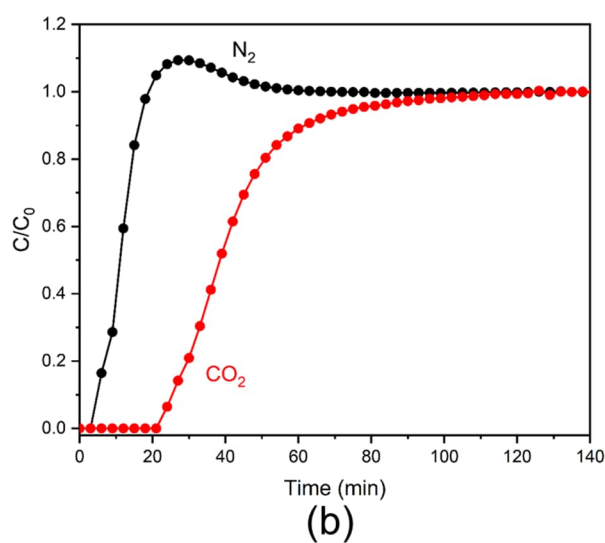
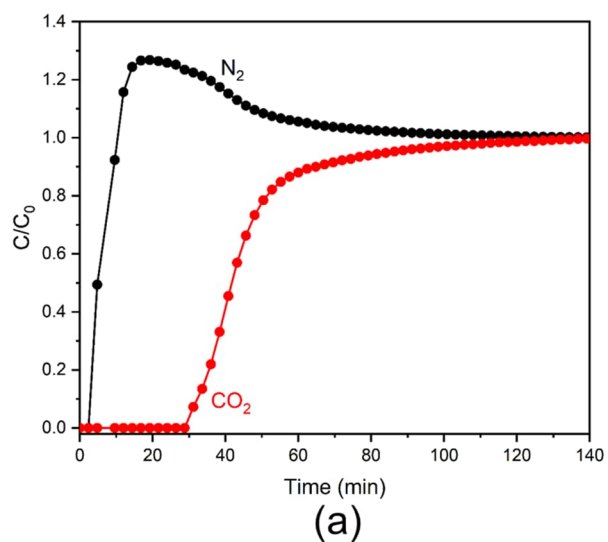


Fig. S8 Breakthrough curves for simulated flue gas (15v% CO₂/85v% N₂) at 293 K and 1 bar using (a) 3,5-DAP-TPA POP, (b) 3,5-DAP-IPA POP, and (c) 3,5-DAP-BDA POP. 1 g of each POP sample and a flow rate of 2 mL/min were used for the measurements.

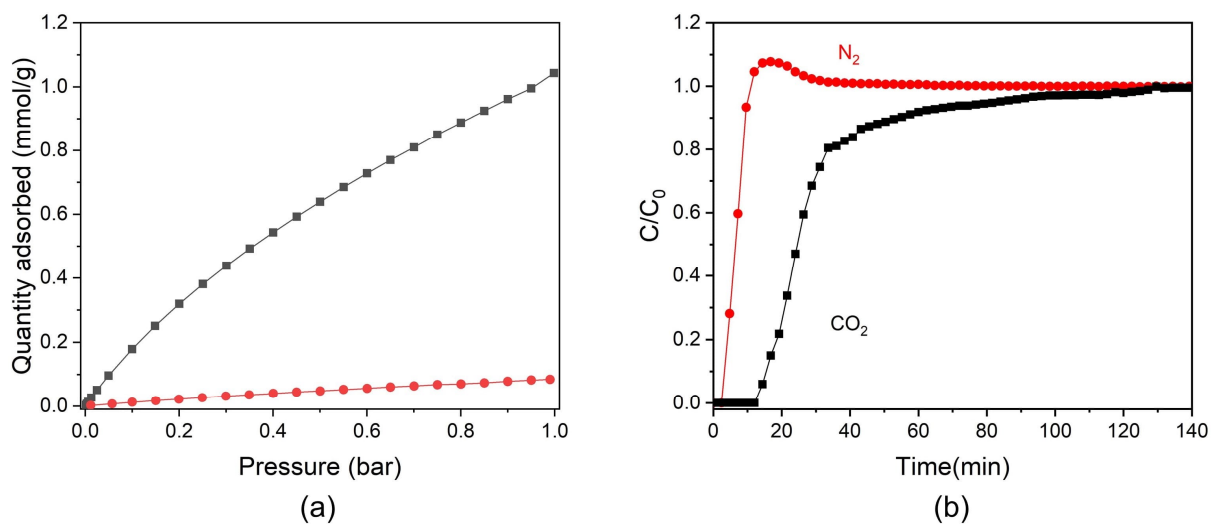


Fig. S9 (a) CO₂ and N₂ adsorption isotherms of LSS-2,6-DAP-TPA POP measured at 313 K and 0–1 bar; (b) breakthrough curves for simulated flue gas (15v% CO₂/85v% N₂) using LSS-2,6-DAP-TPA POP at 313 K and 1 bar. 1 g of the POP sample and a flow rate of 2 mL/min were used for the breakthrough measurement.

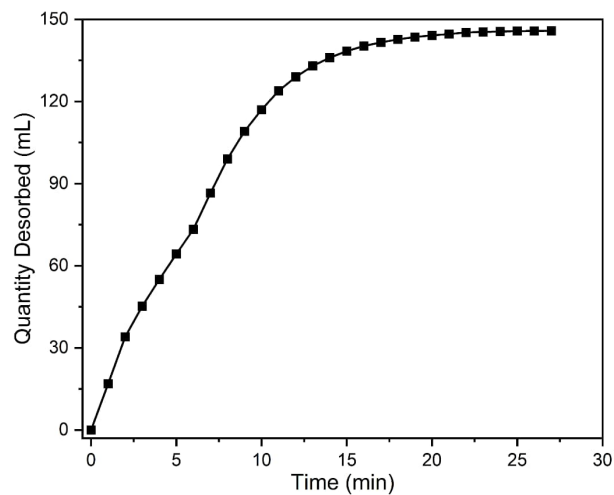


Fig. S10 Desorption kinetics of LSS-2,6-DAP-TPA POP at 150 °C under a reduced pressure.

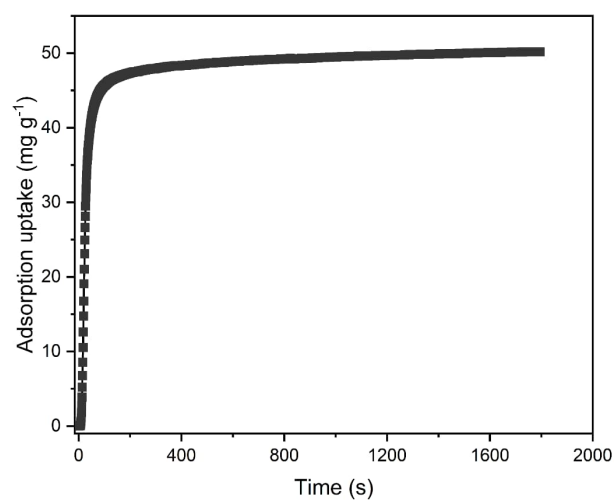


Fig. S11 Kinetics of Gravimetric CO₂ uptake of LSS-2,6-DAP-TPA POP recorded on TGA at 25 °C.

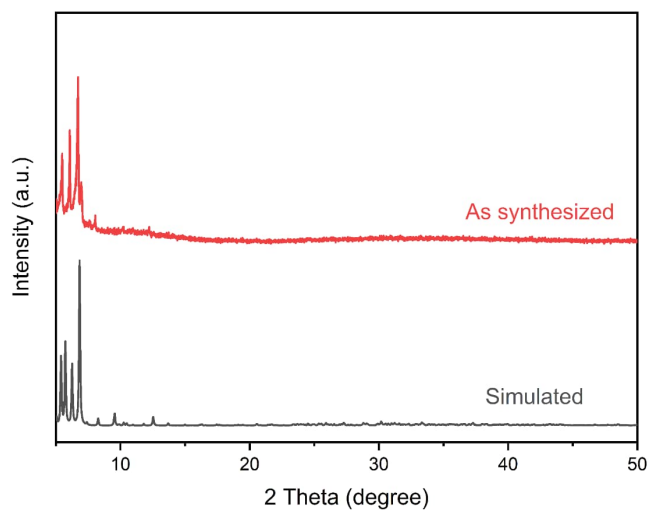


Fig. S12 Comparison of experimental and simulated XRD patterns of Ag₃₃. The slight disagreement between the XRD patterns can be attributed to the weak stability of the cluster under ambient conditions during the XRD measurement. Single-crystal X-ray diffraction analysis confirmed the successful synthesis of Ag₃₃ crystals, revealing a triclinic crystal system with unit cell parameters: $a = 15.479 \text{ \AA}$, $b = 32.705 \text{ \AA}$, $c = 19.035 \text{ \AA}$, $\alpha = 90^\circ$, $\beta = 112.988^\circ$, $\gamma = 90^\circ$, and a unit cell volume of 8871 \AA^3 , which are consistent with previously reported data. ^[1]

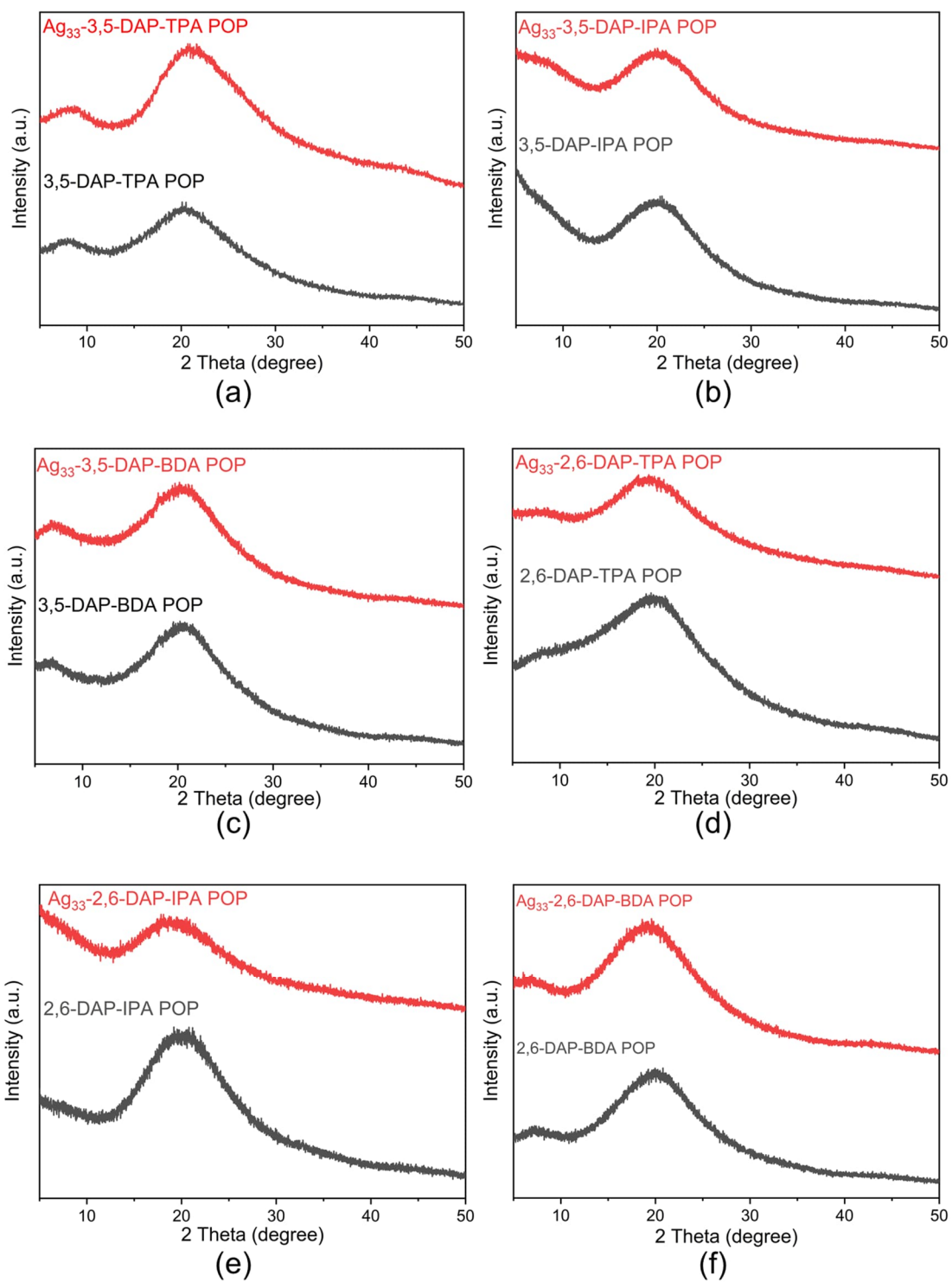


Fig. S13 XRD patterns of the POPs and Ag₃₃-POPs.

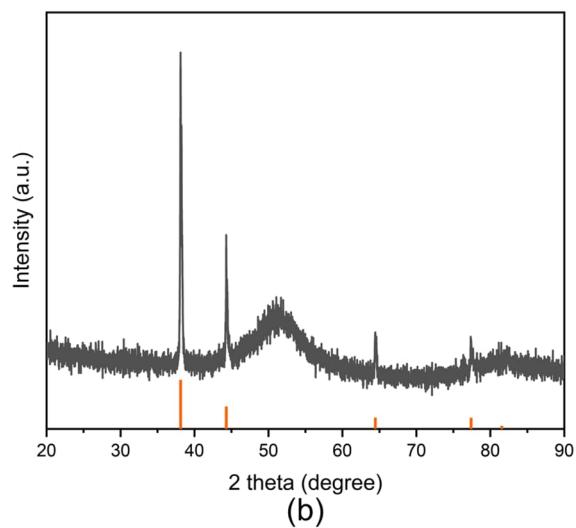
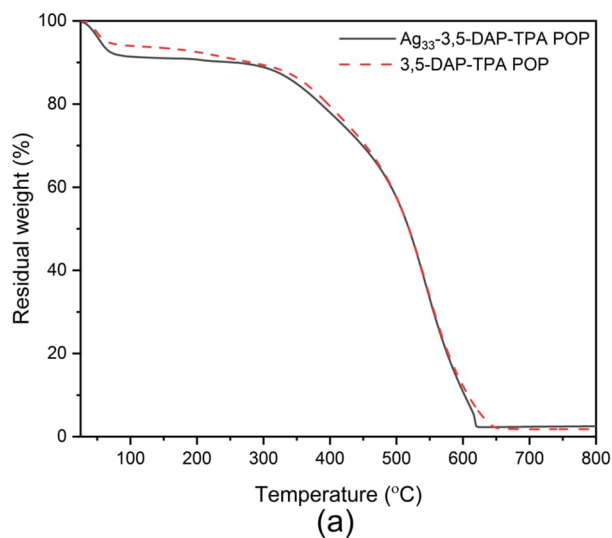


Fig. S14 (a) TGA curves of 3,5-DAP-TPA POP and Ag₃₃-3,5-DAP-TPA POP recorded under an air atmosphere. (b) Comparison of the XRD pattern of the residue of Ag₃₃-3,5-DAP-TPA POP and elemental Ag (ICDD reference code: 04-003-7259), indicating the presence of elemental Ag in the residue.

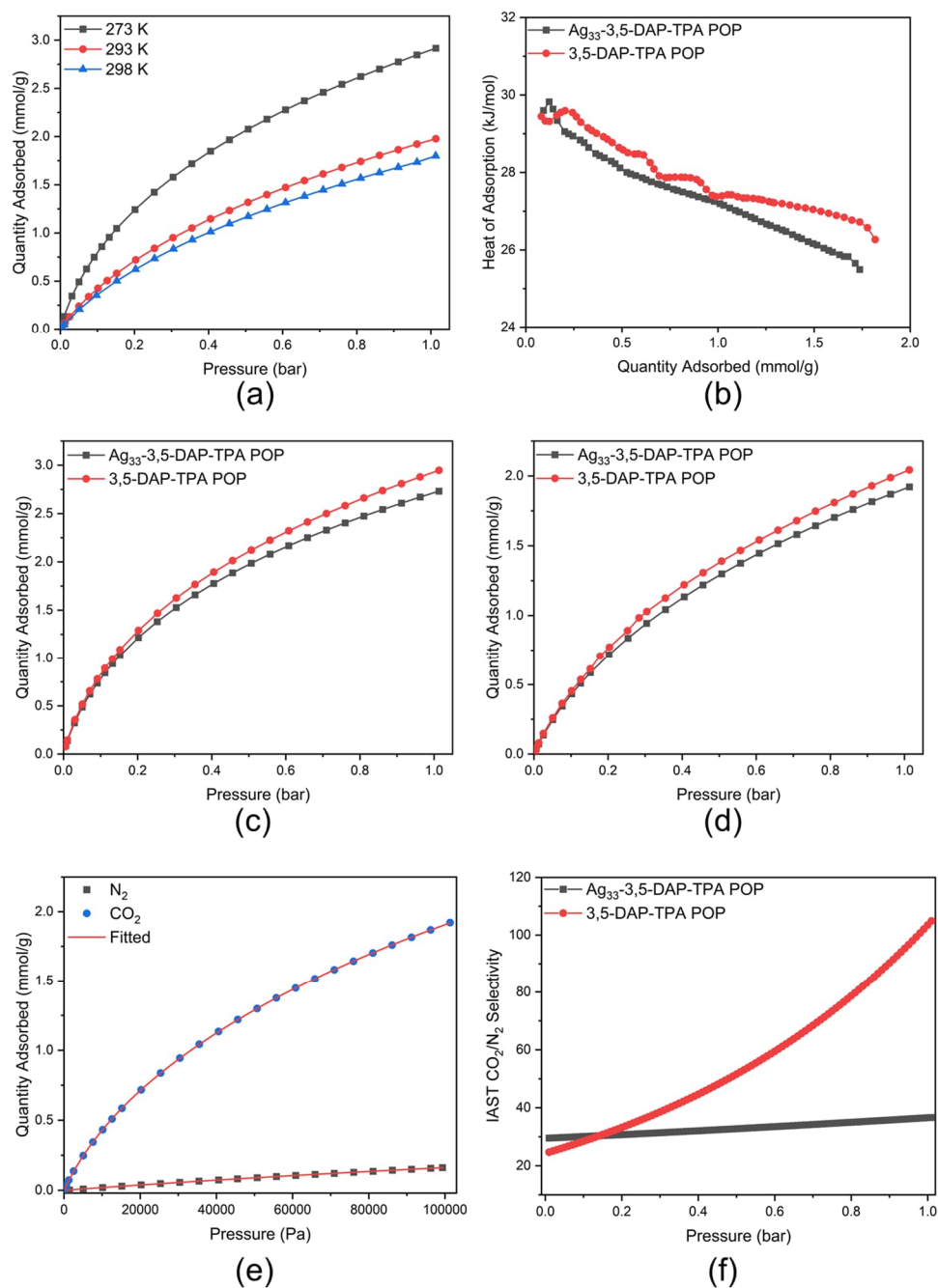


Fig. S15 (a) CO₂ adsorption isotherms of Ag₃₃-3,5-DAP-TPA POP recorded at 273, 293, and 298 K. (b) A comparison of heat of adsorption of CO₂ for 3,5-DAP-TPA POP and Ag₃₃-3,5-DAP-TPA POP. A comparison of CO₂ adsorption isotherm of 3,5-DAP-TPA POP and Ag₃₃-3,5-DAP-TPA POP at 273 K(c) and 293 K (d). (e) A comparison of CO₂ and N₂ adsorption isotherms of Ag₃₃-3,5-DAP-TPA POP recorded at 293 K. The red curves show the fitted results. CO₂ adsorption isotherm was fitted by dual-site Langmuir model, while N₂ adsorption isotherm was fitted by single site Langmuir model. The fitted results are presented in Table S7. (f) CO₂-over-N₂ selectivity of 3,5-DAP-TPA POP and Ag₃₃-3,5-DAP-TPA POP for a simulated gas mixture consisting of 15v% CO₂ and 85v% N₂ at 293 K.

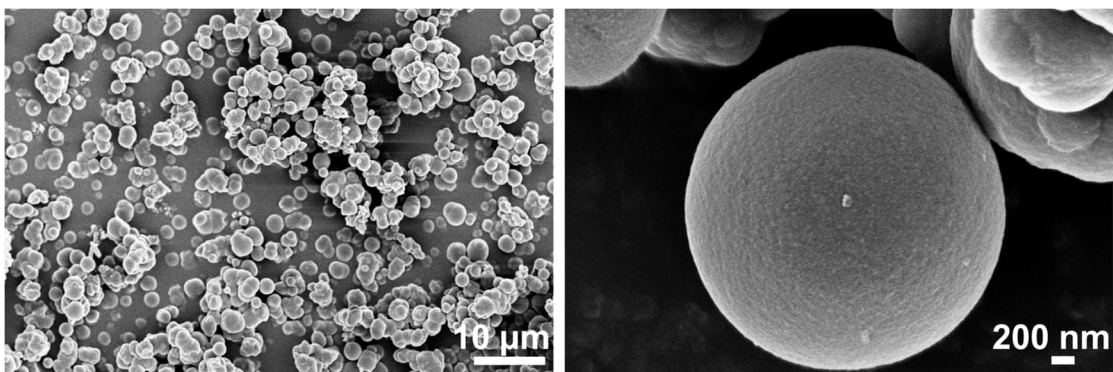


Fig. S16 SEM images of 3,5-DAP-TPA POP.

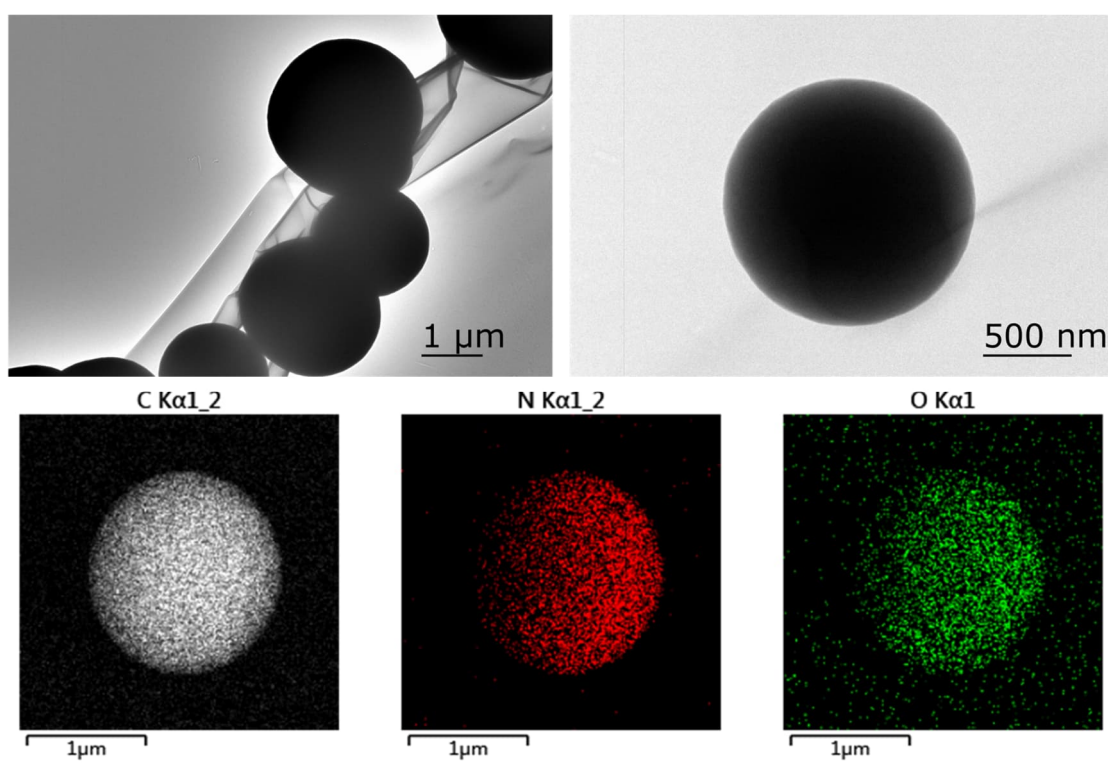


Fig. S17 TEM images and EDS elemental mapping images of 3,5-DAP-TPA POP.

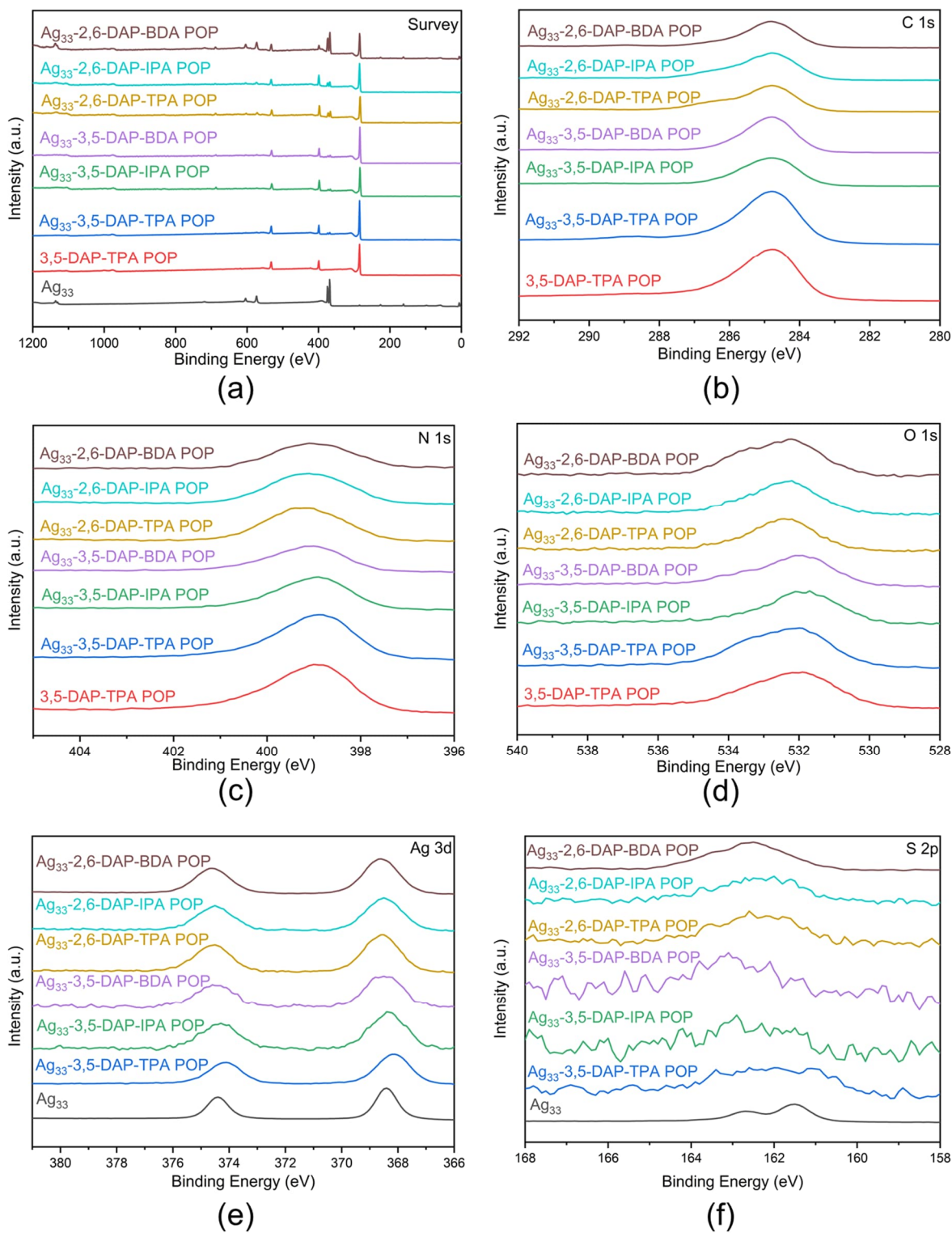


Fig. S18 XPS spectra of Ag_{33} , POPs and Ag_{33} -POPs.

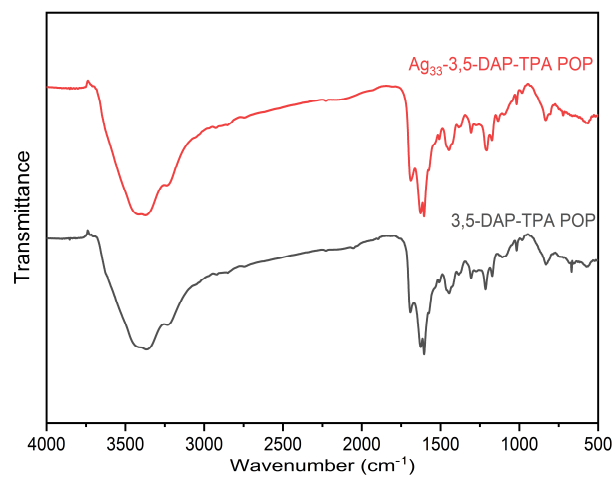
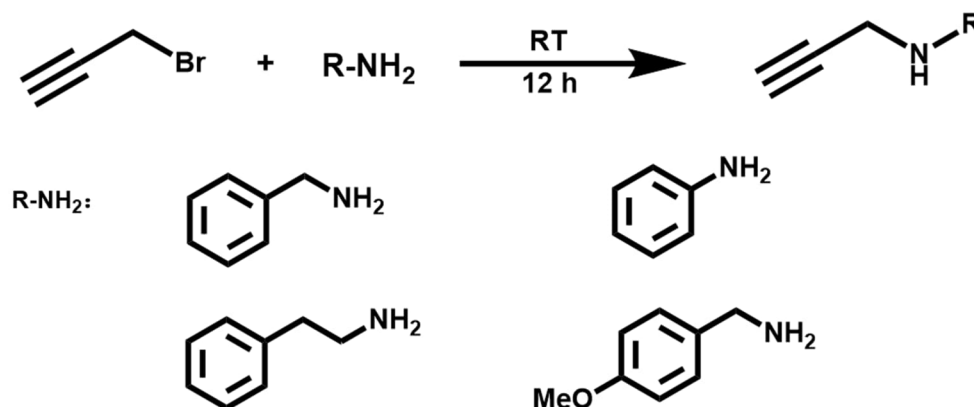


Fig. S19 Infrared spectra of 3,5-DAP-TPA POP and Ag_{33} -3,5-DAP-TPA POP.

Catalysis

Synthesis of substrates [4]

In a typical experiment, propargylic bromide (1 mL, 13.3 mmol) was slowly added to a 50 mL round-bottom flask containing propargylamine (54 mmol) over 30 min at 0 °C. Subsequently, the resulting mixture was stirred at room temperature for 12 h. The mixture was then diluted with ether and washed with saturated NaHCO₃ aqueous solution (3×30 mL). The organic phase was dried over anhydrous Na₂SO₄, filtered, and the solvent was evaporated under reduced pressure. The crude product was purified by column chromatography using a petroleum ether/ethyl acetate (10:1) mixture, giving the pure product of propargylic amine as a yellow liquid.

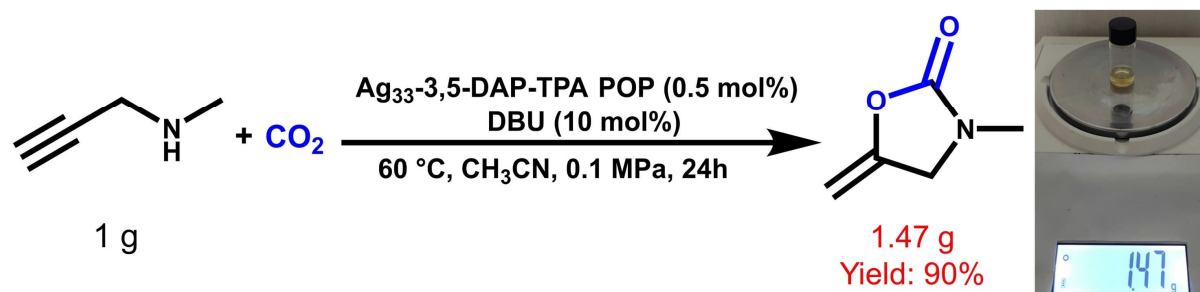


Scheme S1. General procedure for the synthesis of terminal propargylic amine.

General procedure for the Ag₃₃-POP-catalyzed CO₂ cycloaddition with propargylamine

A Schlenk flask was charged with Ag₃₃-POP (0.004 mmol based on Ag), propargylamine (0.8 mmol), 1,8-diazabicyclo[5.4.0]undec-7-ene (DBU, 12.2 mg, 0.08 mmol), and solvent (6 mL). The flask was then connected to a balloon filled with CO₂ and stirred at the desired temperature (25 or 60 °C) for the desired time (1–24 h). The heterogeneous catalyst was removed through centrifugation, and the solid was thoroughly washed with CH₃CN. The resulting CH₃CN solution was combined with the supernatant obtained from centrifugation. The combined mixture was subjected to rotary evaporation, and the obtained crude product was further purified by flash chromatography on silica using dichloromethane/petroleum ether (v/v = 20/1) as the eluent, affording the pure products.

Procedure for the gram-scale Ag₃₃-3,5-DAP-TPA POP-catalyzed CO₂ cycloaddition with propargylamine



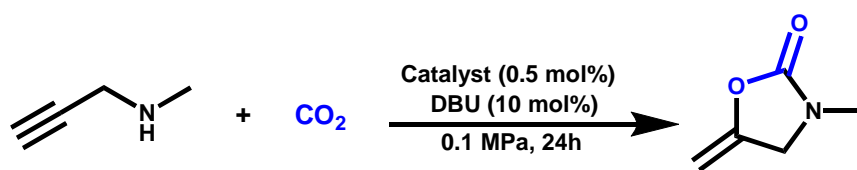
Scheme S2. Gram scale reaction of CO₂ cycloaddition with *N*-methylpropargylamine catalyzed by Ag₃₃-3,5-DAP-TPA POP.

A Schlenk flask was charged with Ag₃₃-3,5-DAP-TPA POP (316 mg, 2.47 wt.% Ag), *N*-methylpropargylamine (1.0 g, 14.47 mmol), DBU (220.3 mg, 1.447 mmol), and CH₃CN (100 mL). The flask was then connected to a balloon filled with CO₂ and stirred at 60 °C for 24 h. The heterogeneous catalyst was removed through centrifugation, and the solid was thoroughly washed with CH₃CN. The resulting CH₃CN solution was combined with the supernatant obtained from centrifugation. The combined mixture was subjected to rotary evaporation, and the obtained crude product was further purified by flash chromatography on silica using dichloromethane/petroleum ether (v/v = 20/1) as the eluent, affording the pure product **2a** (Yield: 90%, 1.47 g).

General procedure for sequential CO₂ capture and conversion process

As depicted in Fig. 6a-b, a 150 mL round-bottom flask was utilized as the catalytic reactor. It was loaded with Ag₃₃-3,5-DAP-TPA POP (17.5 mg, 0.5 mol%) and connected to the pilot-scale breakthrough setup. The flask was evacuated using a vacuum pump. By switching Valve 5, the catalytic reactor was linked to the gas collection bottle, allowing the captured CO₂ to be transferred into the reactor. Once the gas transfer was completed, Valve 5 was switched again to disconnect the catalytic reactor from the gas collection bottle. A mixture of CH₃CN (6 mL), *N*-methylpropargylamine (**1a**), and DBU was then injected into the catalytic reactor via a syringe. The reaction mixture was stirred at 60 °C for 6 hours. After the reaction, the heterogeneous catalyst was removed by centrifugation, and the solid residue was thoroughly washed with CH₃CN. The CH₃CN solution was combined with the supernatant from the centrifugation, and the mixture was subjected to rotary evaporation. The crude product obtained was further purified using flash chromatography on silica with a dichloromethane/petroleum ether mixture (v/v = 20/1) as the eluent, yielding pure product of **2a**. The catalytic results are presented in Table S13.

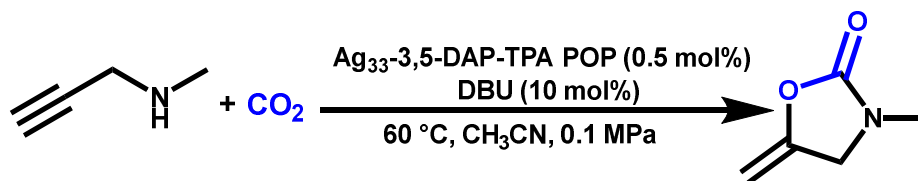
By repeating the catalytic reactions that convert captured CO₂ from simulated flue gas, a sustained conversion of flue gas into fine chemicals was achieved.

Table S9 Control Experiments for Chemical Conversion of *N*-methylpropargylamine with CO₂

Entry ^a	catalyst	Temperature (°C)	Solvent	Yield (%)
1	Ag ₃₃ -3,5-DAP-TPA POP	RT	CH ₃ OH	50
2	Ag ₃₃ -3,5-DAP-TPA POP	RT	THF	40
3	Ag ₃₃ -3,5-DAP-TPA POP	RT	DMF	70
4	Ag ₃₃ -3,5-DAP-TPA POP	RT	CH ₃ CN	80
5	Ag ₃₃ -3,5-DAP-TPA POP	60 °C	CH ₃ CN	95
6	3,5-DAP-TPA POP	60 °C	CH ₃ CN	9
7	^t BuSAg	60 °C	CH ₃ CN	32
8	CF ₃ COOAg	60 °C	CH ₃ CN	29
9	Ag ₃₃	60 °C	CH ₃ CN	53
10	Ag ₃₃ -3,5-DAP-IPA POP	60 °C	CH ₃ CN ^b	87
11	Ag ₃₃ -3,5-DAP-BDA POP	60 °C	CH ₃ CN	89
12	Ag ₃₃ -2,6-DAP-TPA POP	60 °C	CH ₃ CN	88
13	Ag ₃₃ -2,6-DAP-IPA POP	60 °C	CH ₃ CN	83
14	Ag ₃₃ -2,6-DAP-BDA POP	60 °C	CH ₃ CN	85

^a *N*-Methylpropargylamine (0.8 mmol), DBU (12.2 mg, 0.08 mmol), solvent (6 mL); ^b solvent: 8 mL CH₃CN

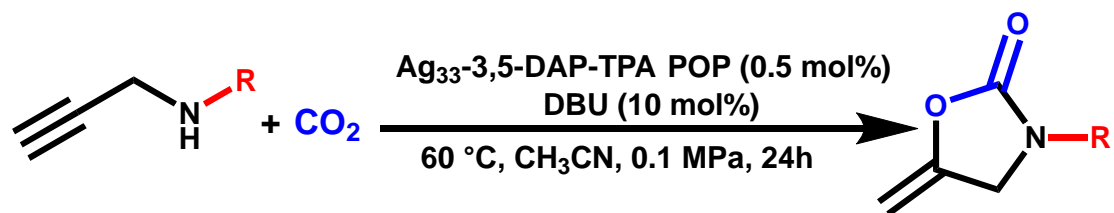
Table S10 Influence of partial pressure of CO₂ on its cycloaddition with *N*-Methylpropargylamine catalyzed by Ag₃₃-3,5-DAP-TPA POP



Entry	CO ₂ partial pressure (MPa) ^a	Time (h)	Yield(%)
1	0	6	0
2	0.015	6	66
3	0.05	6	82
4	0.07	6	92
5	0.09	6	93
6	0.1	6	93

^a The total gas pressure is 1 bar and the partial pressure of CO₂ was controlled by mixing CO₂ with specific amount of N₂.

Table S11 Catalytic results of CO₂ cycloaddition with various propargylamines using Ag₃₃-3,5-DAP-TPA POP



Entry	Substrates	Products	Yield (%)
1			95
2			93
3			90
4			92
5			92

Table S12 The use of silver cluster and POP based catalysts for CO₂ cycloaddition reactions

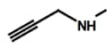
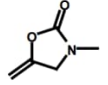
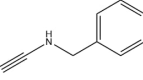
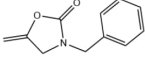
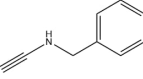
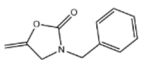
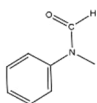
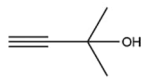
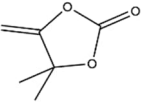
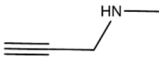
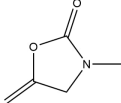
Catalyst	Substrate	Solvent	CO ₂ (atm)	Product	Time (h)	Temp. (°C)	Yield (%)	Ref.
Ag ₃₃ -3,5-DAP-TPA POP		MeCN	1		6	60	93	This work
Ag ₄		MeCN	1		2	25	99	16
Au@Ag ₂₄	R-C≡C-	DMF	1	R-C≡C-COOH	12	50	92	17
Ag ₂₇ -MOF		MeCN	1		6	R. T.	97	18
Zn-TpPa		DMF	1		18	30	99	19
Ag@RB-POP		MeCN	1		12	30	94	20
Pd@BBA-2		DMSO	1		0.5	40	98	21

Table S13 The catalytic results of continuous sequential CO₂ capture and conversion processes

Entry	Conditions of Breakthrough experiment		Catalytic conditions		Yield (%)	Space-time Yield (kg/m ³ _{POP} /day)
	Simulated flue gas	Flow rate (mL/min)	Reactant	Reaction time (h)		
1	15v% CO ₂ /85v% N ₂	2	0.8 mmol 1a 0.08 mmol DBU	6	89	5.8
2	15v% CO ₂ /85v% N ₂ +50 ppm NO ₂ + 50 ppm SO ₂	2	0.8 mmol 1a 0.08 mmol DBU	6	88	5.7
3	15v% CO ₂ /85v% N ₂	10	0.8 mmol 1a 0.08 mmol DBU	6	86	5.6
4	15v% CO ₂ /85v% N ₂	10	1.6 mmol 1a 0.16 mmol DBU	6	74	9.6

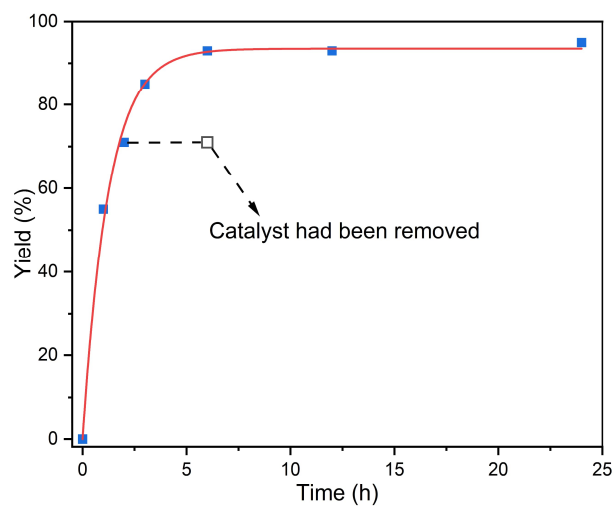


Fig. S19 Result of hot filtration experiment for the cycloaddition reaction of *N*-methylpropargylamine with CO₂ catalyzed by Ag₃₃-3,5-DAP-TPA POP.

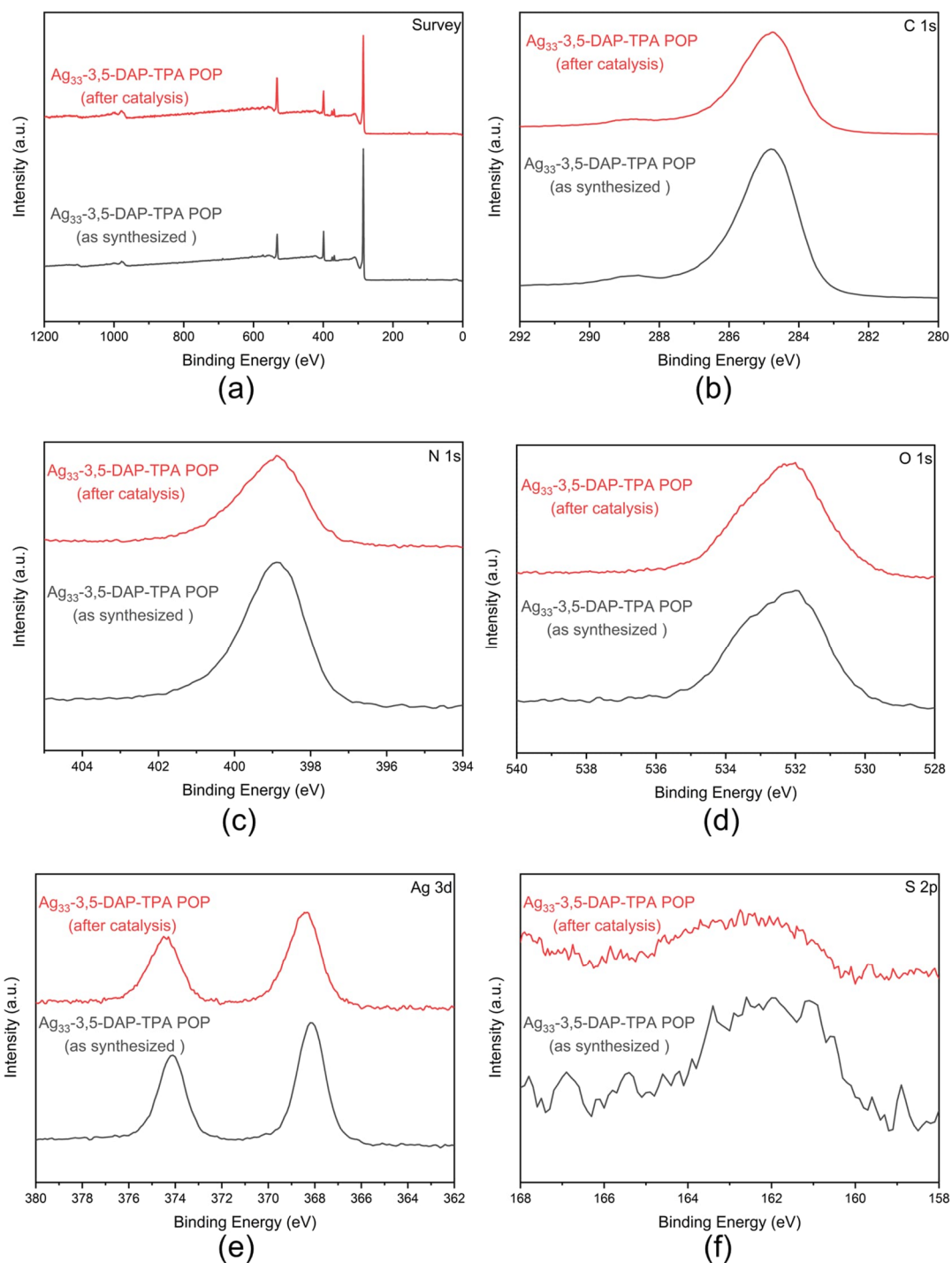


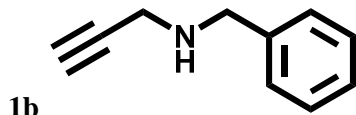
Fig S20 Comparison XPS spectra of the as synthesized catalyst $\text{Ag}_{33}\text{-3,5-DAP-TPA POP}$ and the recovered catalyst after the catalysis reactions.

NMR data



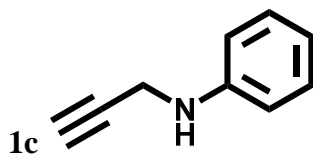
^1H NMR (400 MHz, Chloroform-*d*) δ 3.30 (d, $J = 2.5$ Hz, 2H), 2.39 (s, 3H), 2.16 (t, $J = 2.4$ Hz, 1H), 1.37 (br s, 1H)

^{13}C NMR (101 MHz, Chloroform-*d*) δ 81.92, 71.40, 39.87, 39.56, 35.12



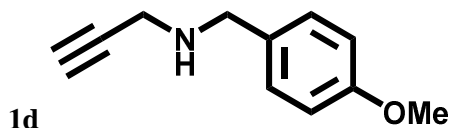
^1H NMR (400 MHz, Chloroform-*d*) δ 7.42–7.24 (m, 5H), 3.90 (s, 2H), 3.45 (d, $J = 2.5$ Hz, 2H), 2.28 (t, $J = 2.4$ Hz, 1H), 1.54 (br s, 1H)

^{13}C NMR (101 MHz, Chloroform-*d*) δ 139.41, 128.48, 128.45, 127.20, 82.10, 71.61, 52.29, 37.35



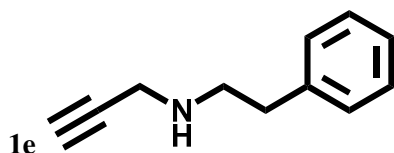
^1H NMR (400 MHz, Chloroform-*d*) δ 7.29–7.22 (m, 2H), 6.84 (t, $J = 7.3$ Hz, 1H), 6.72 (d, $J = 7.5$ Hz, 2H), 3.96 (d, $J = 2.5$ Hz, 2H), 2.26 (t, $J = 2.4$ Hz, 1H)

^{13}C NMR (101 MHz, Chloroform-*d*) δ 146.91, 129.31, 118.69, 113.59, 81.12, 71.37, 33.67



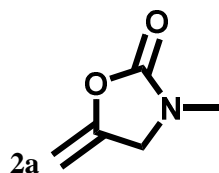
^1H NMR (400 MHz, Chloroform-*d*) δ 7.25 (d, $J = 8.9$ Hz, 2H), 6.86 (d, $J = 8.7$ Hz, 2H), 3.80 (s, 2H), 3.78 (s, 3H), 3.39 (d, $J = 2.5$ Hz, 2H), 2.25 (t, $J = 2.4$ Hz, 1H), 1.60 (br s, 1H)

^{13}C NMR (101 MHz, Chloroform-*d*) δ 158.80, 131.49, 129.65, 113.83, 82.15, 71.56, 55.25, 51.64, 37.16



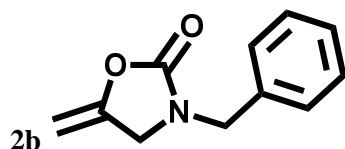
^1H NMR (400 MHz, Chloroform-*d*) δ 7.38–7.22 (m, 5H), 3.48 (d, $J = 2.4$ Hz, 2H), 3.02 (t, $J = 6.8$ Hz, 2H), 2.86 (t, $J = 7.1$ Hz, 2H), 2.24 (t, $J = 2.4$ Hz, 1H), 1.35 (br s, 1H)

^{13}C NMR (101 MHz, Chloroform-*d*) δ 139.77, 128.73, 128.52, 126.26, 82.05, 71.42, 49.77, 38.12, 36.15



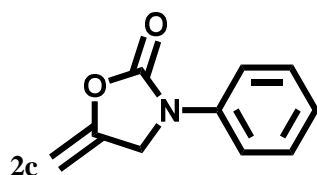
$^1\text{H NMR}$ (400 MHz, Chloroform-*d*) δ 4.68 (d, $J = 2.8$ Hz, 1H), 4.25 (d, $J = 2.6$ Hz, 1H), 4.13 (t, $J = 2.5$ Hz, 2H), 2.88 (s, 3H)

$^{13}\text{C NMR}$ (101 MHz, Chloroform-*d*) δ 155.76, 148.92, 86.36, 49.89, 30.39



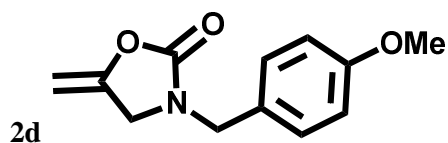
$^1\text{H NMR}$ (400 MHz, Chloroform-*d*) δ 7.42–7.25 (m, 5H), 4.75 (d, $J = 2.8$ Hz, 1H), 4.48 (s, 2H), 4.25 (d, $J = 3.2$ Hz, 1H), 4.03 (t, $J = 2.4$ Hz, 2H)

$^{13}\text{C NMR}$ (101 MHz, Chloroform-*d*) δ 155.66, 148.95, 134.98, 128.99, 128.27, 128.19, 86.78, 47.87, 47.23



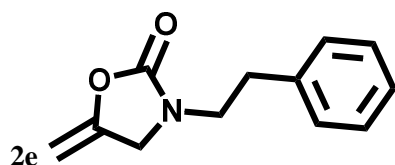
$^1\text{H NMR}$ (400 MHz, Chloroform-*d*) δ 7.54 (d, $J = 7.7$ Hz, 2H), 7.39 (t, $J = 8.0$ Hz, 2H), 7.17 (t, $J = 7.4$ Hz, 1H), 4.85 (d, $J = 2.9$ Hz, 1H), 4.64 (s, 2H), 4.44 (d, $J = 2.6$ Hz, 1H)

$^{13}\text{C NMR}$ (101 MHz, Chloroform-*d*) δ 152.38, 147.67, 137.16, 129.29, 124.58, 118.08, 87.21, 48.41



$^1\text{H NMR}$ (400 MHz, Chloroform-*d*) δ 7.19 (d, $J = 8.2$ Hz, 2H), 6.87 (d, $J = 8.7$ Hz, 2H), 4.71 (d, $J = 2.9$ Hz, 1H), 4.39 (s, 2H), 4.22 (d, $J = 2.3$ Hz, 1H), 3.99 (t, $J = 2.4$ Hz, 2H), 3.79 (s, 3H)

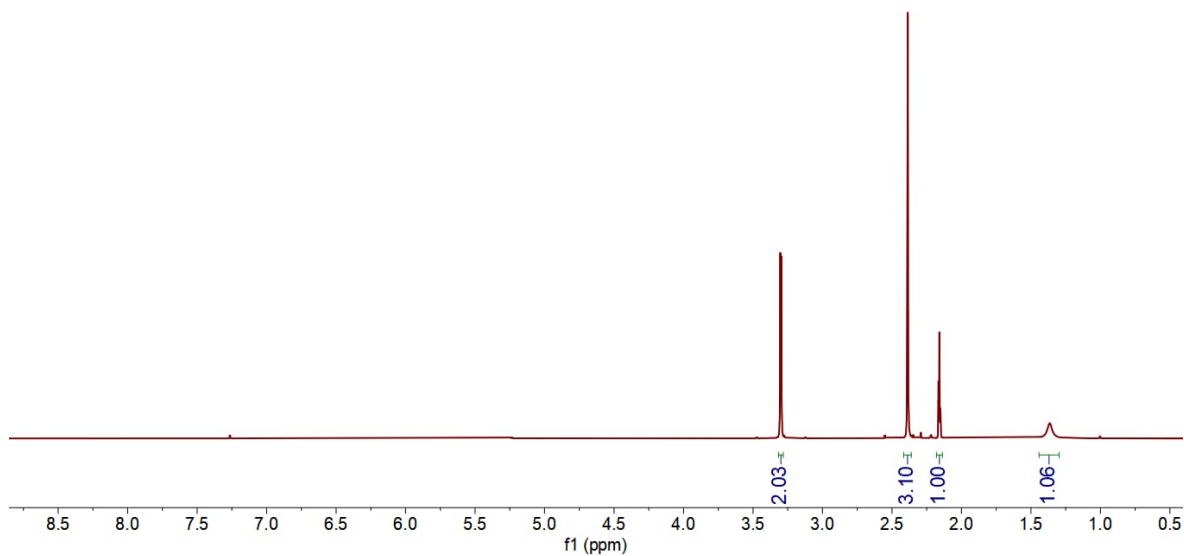
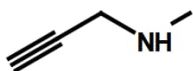
$^{13}\text{C NMR}$ (101 MHz, Chloroform-*d*) δ 159.55, 155.57, 149.07, 129.60, 126.99, 114.30, 86.64, 55.31, 47.22



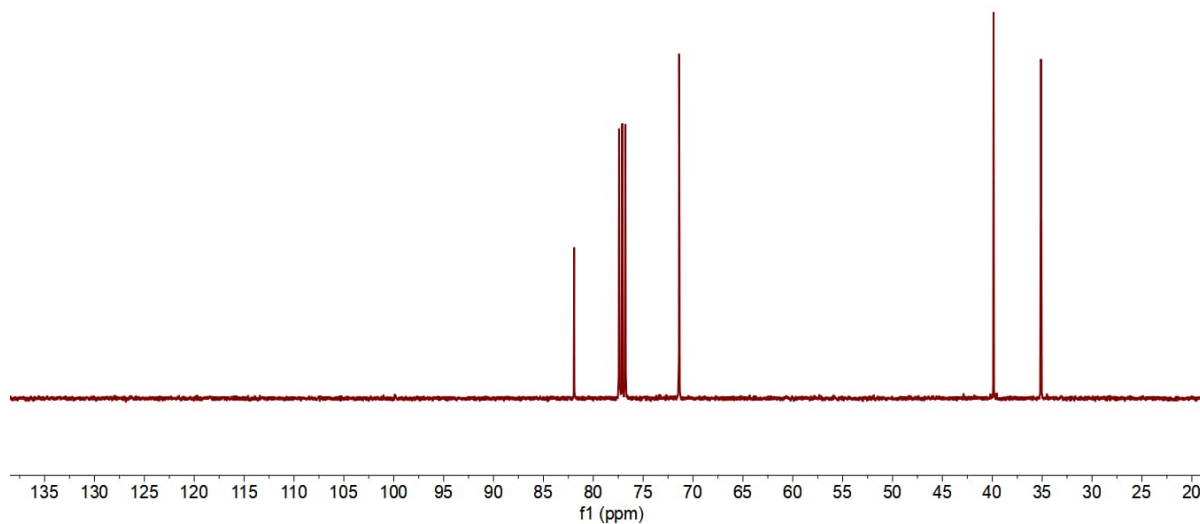
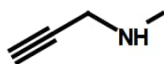
$^1\text{H NMR}$ (400 MHz, Chloroform-*d*) δ 7.32 (t, $J = 7.2$ Hz, 2H), 7.24 (dd, $J = 15.2, 7.1$ Hz, 3H), 4.70 (q, $J = 2.7$ Hz, 1H), 4.22 (d, $J = 3.1$ Hz, 1H), 3.99 (t, $J = 2.4$ Hz, 2H), 3.60–3.53 (m, 2H), 2.89 (t, $J = 7.3$ Hz, 2H)

$^{13}\text{C NMR}$ (101 MHz, Chloroform-*d*) δ 155.47, 149.03, 137.96, 128.79, 128.60, 126.83, 86.47, 48.40, 45.17, 33.93

1a

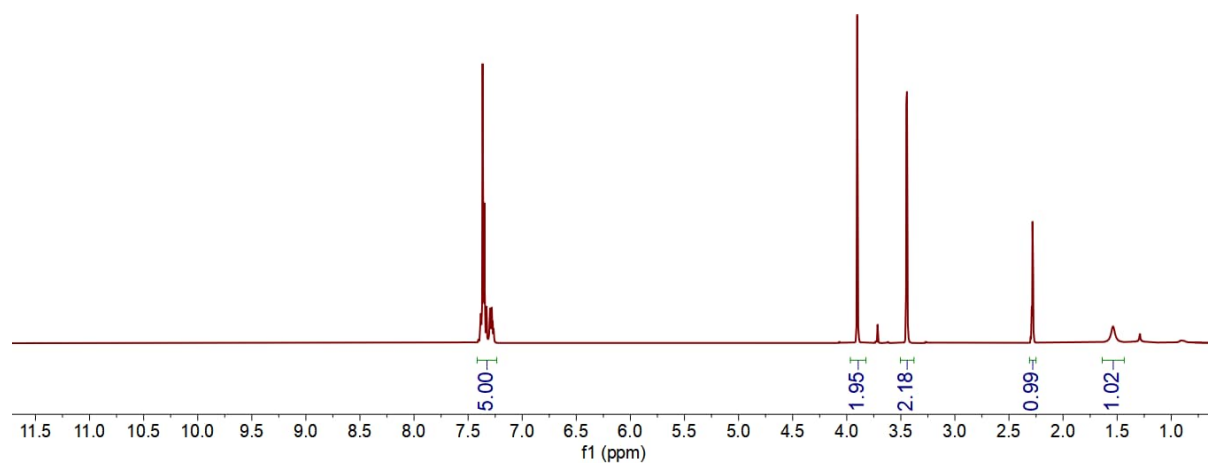
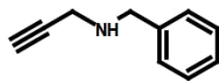


¹H NMR spectrum of 1a

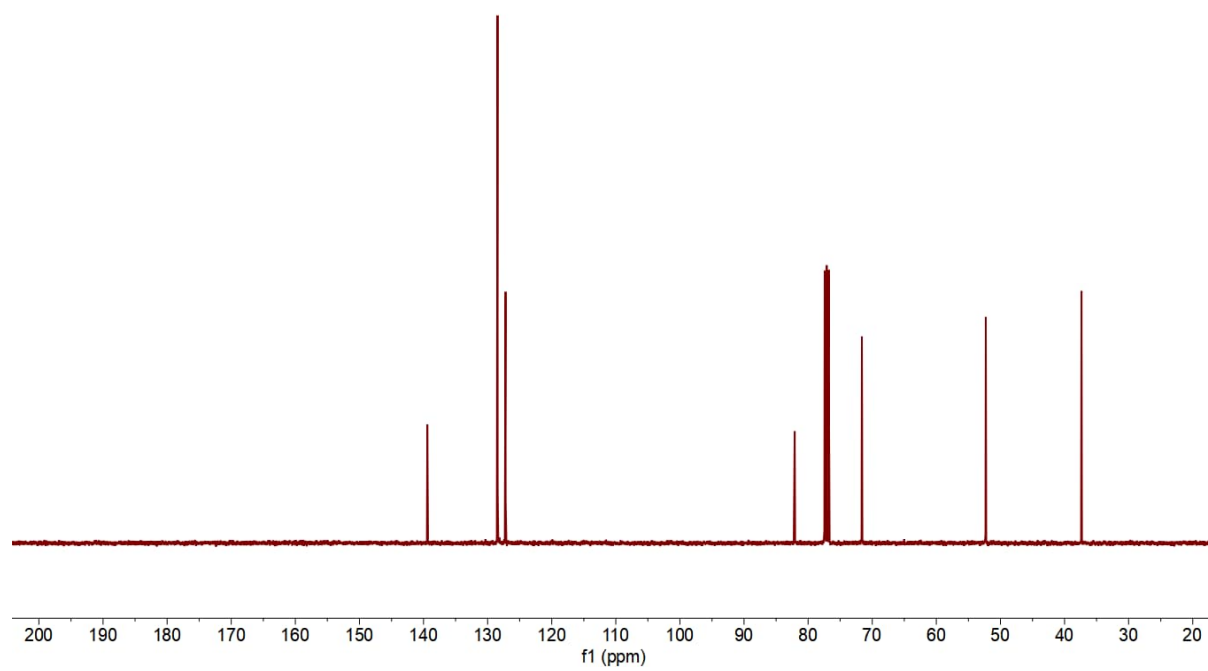
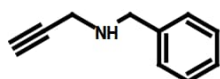


¹³C NMR spectrum of 1a

1b

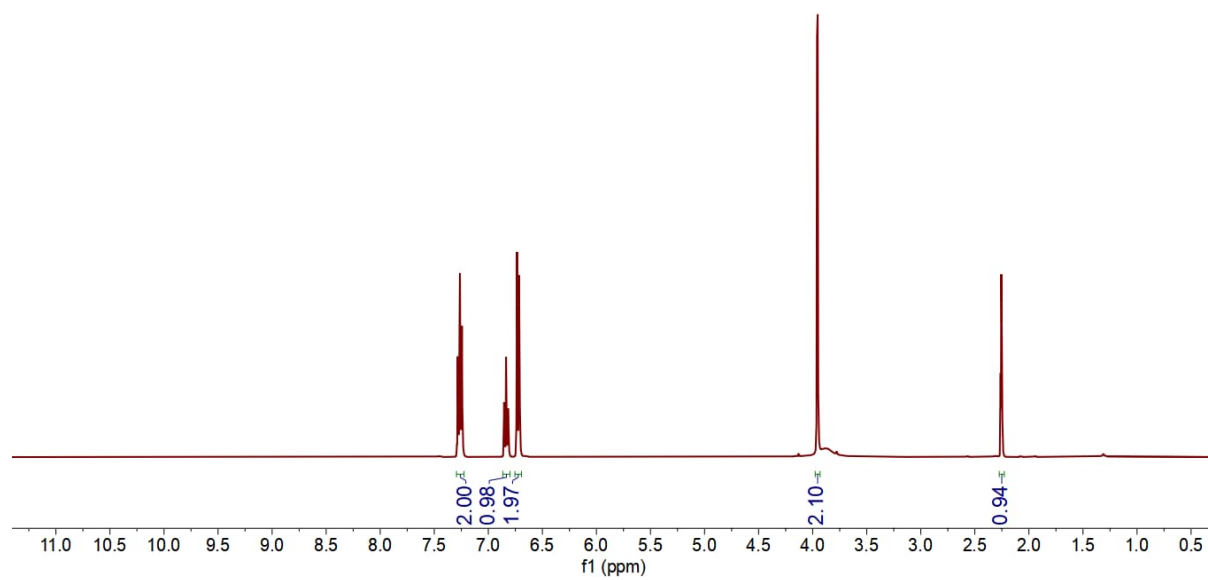
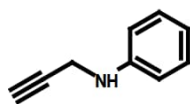


¹H NMR spectrum of **1b**

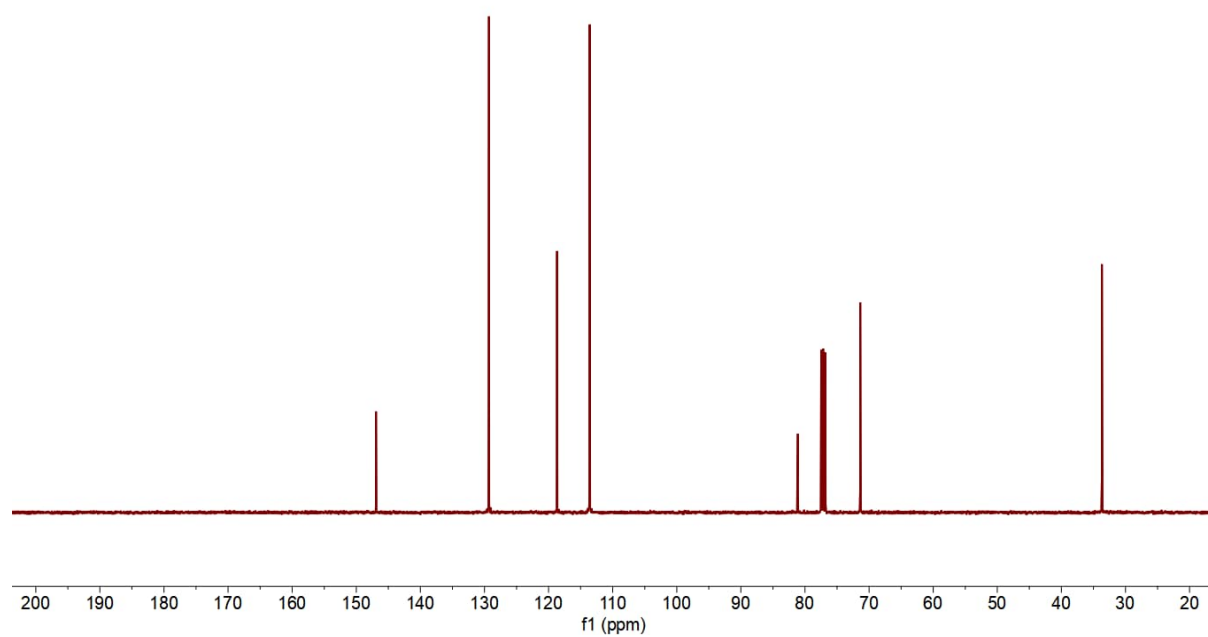
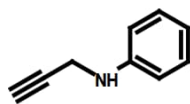


¹³C NMR spectrum of **1b**

1c

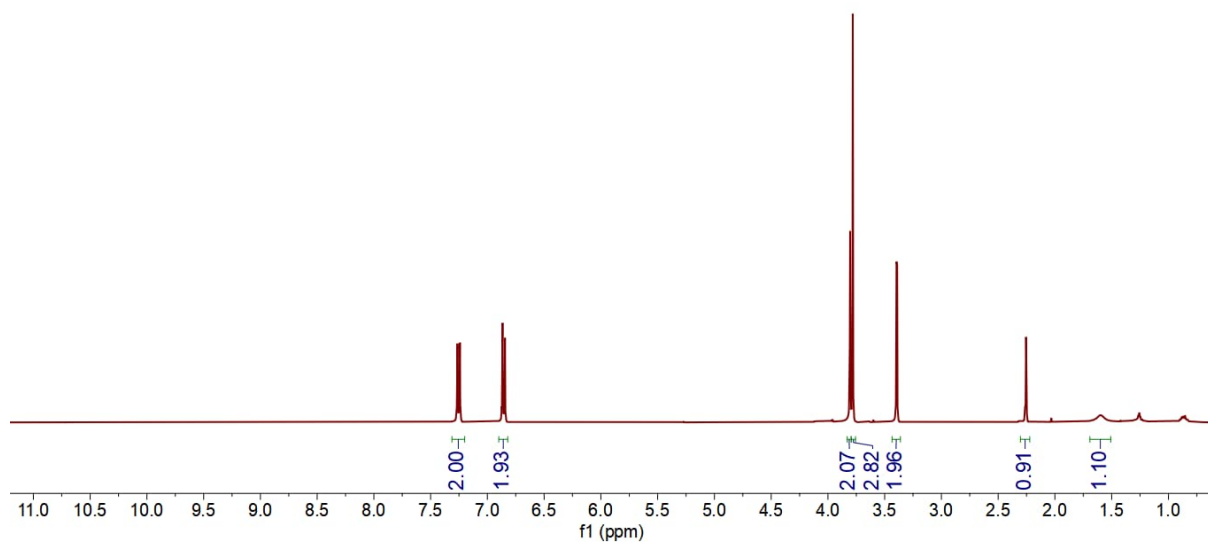
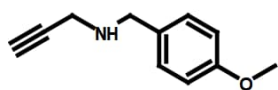


¹H NMR spectrum of 1c

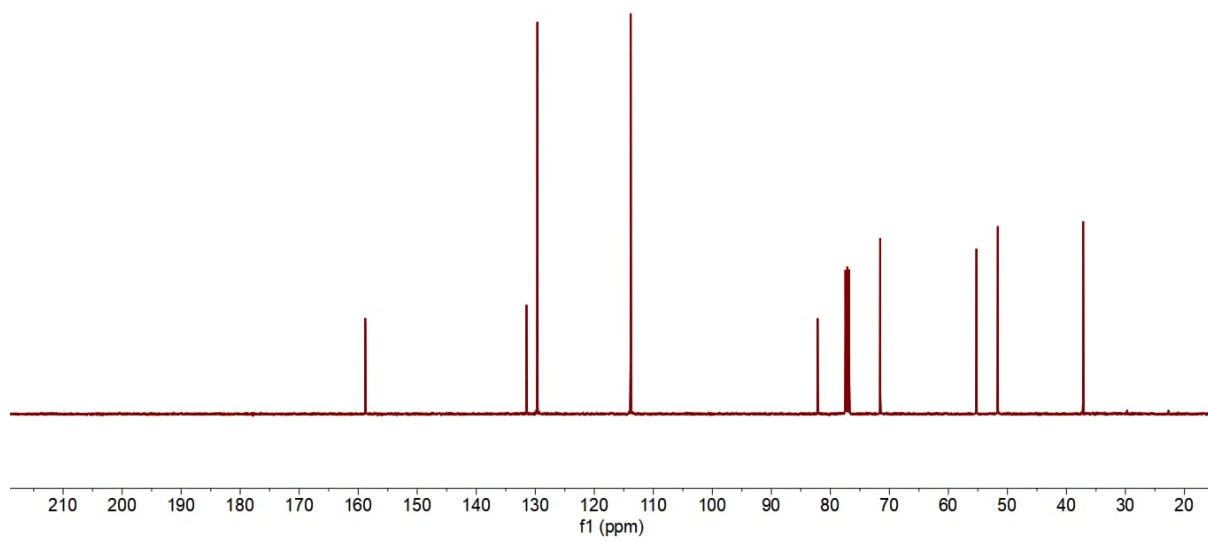
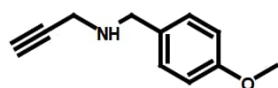


¹³C NMR spectrum of 1c

1d

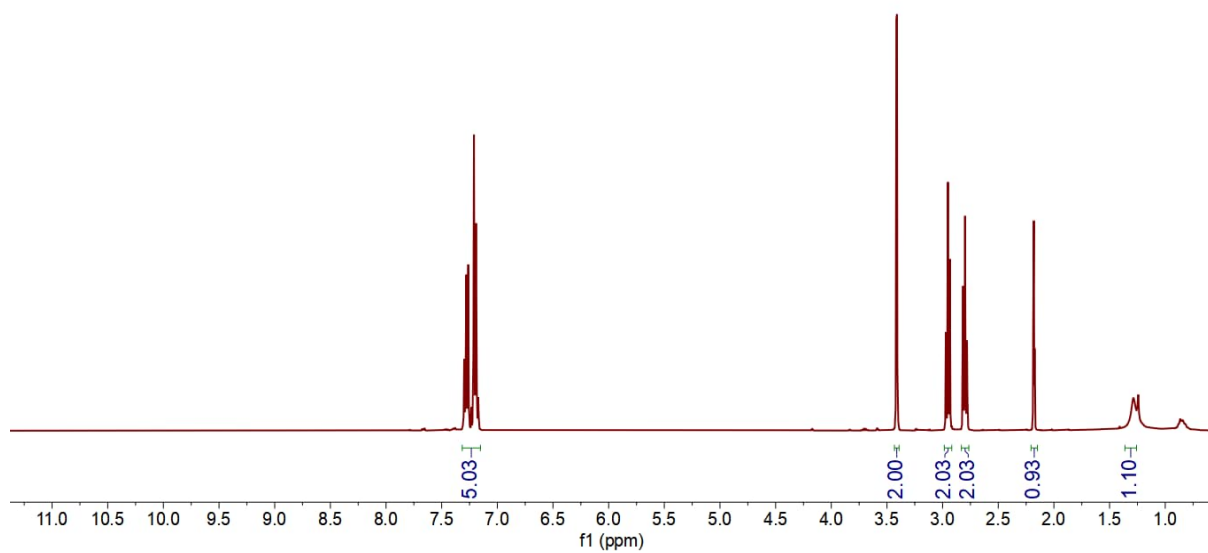
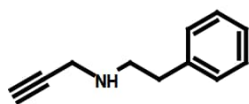


¹H NMR spectrum of **1d**

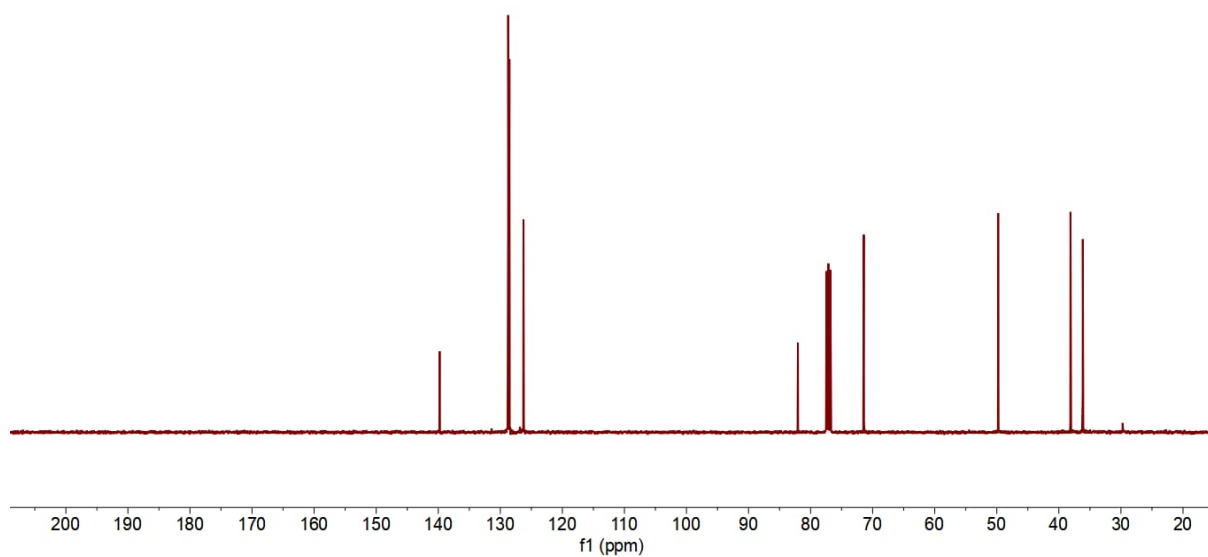
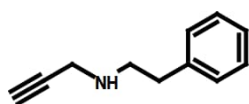


¹³C NMR spectrum of **1d**

1e

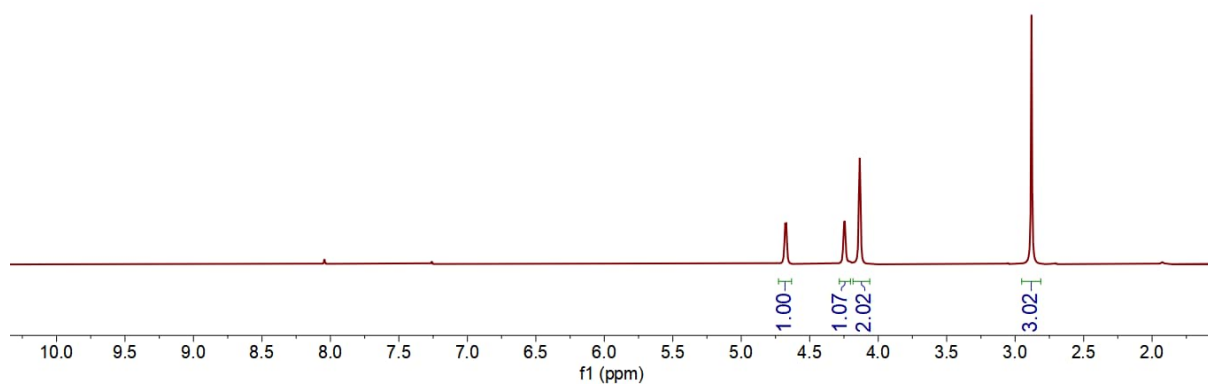
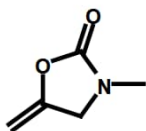


¹H NMR spectrum of **1e**

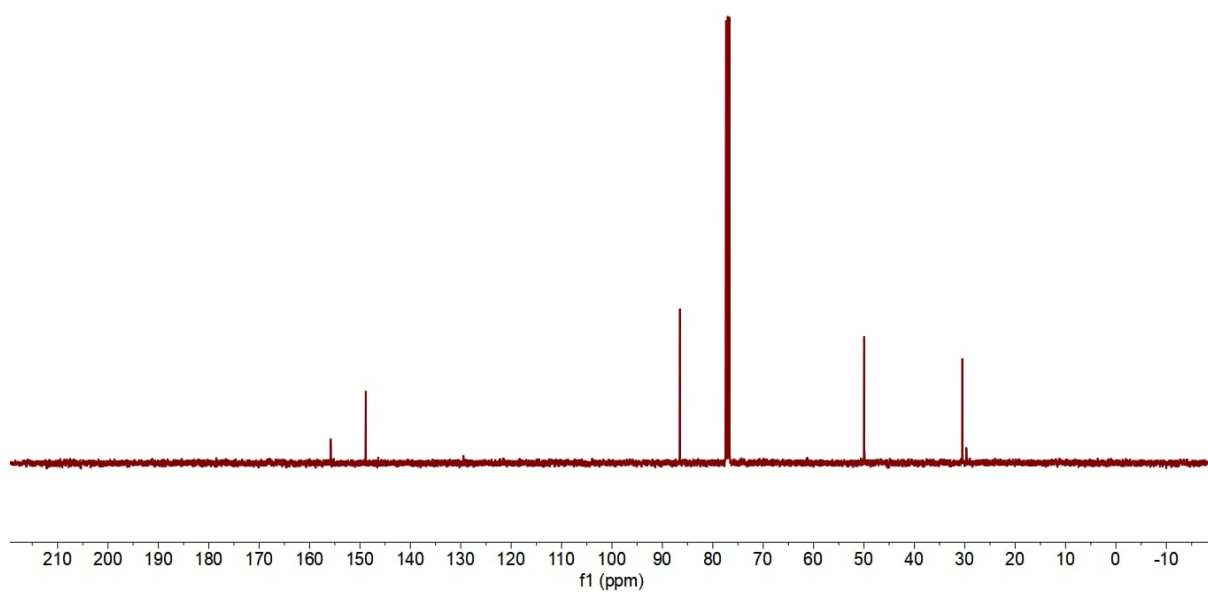
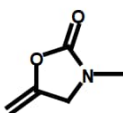


¹³C NMR spectrum of **1e**

2a

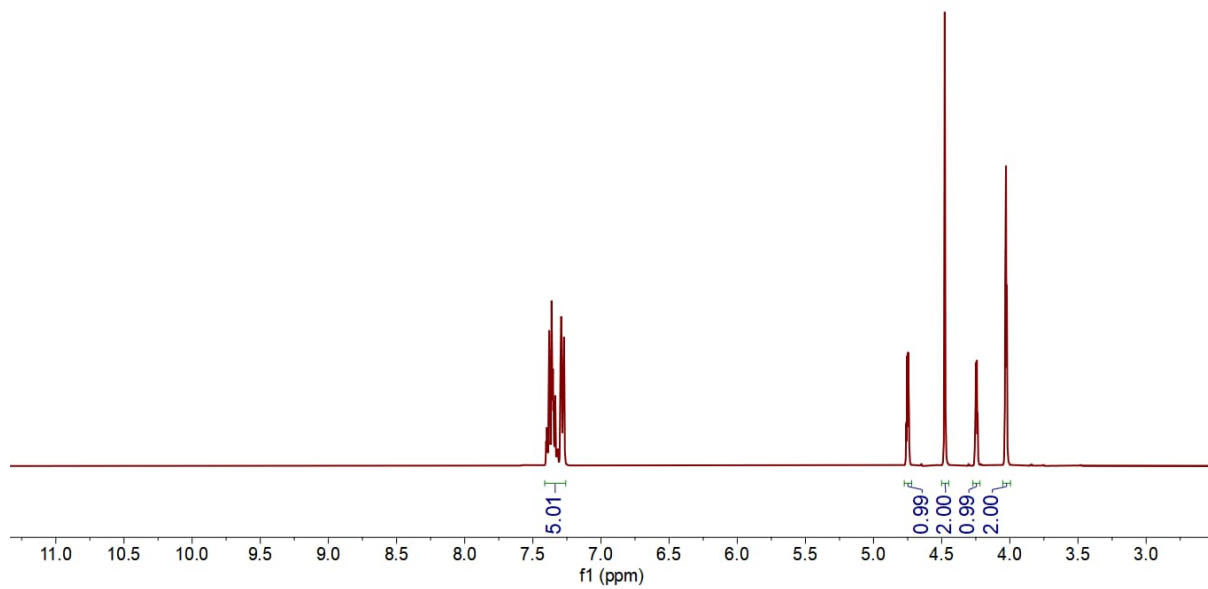
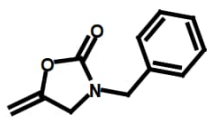


¹H NMR spectrum of 2a

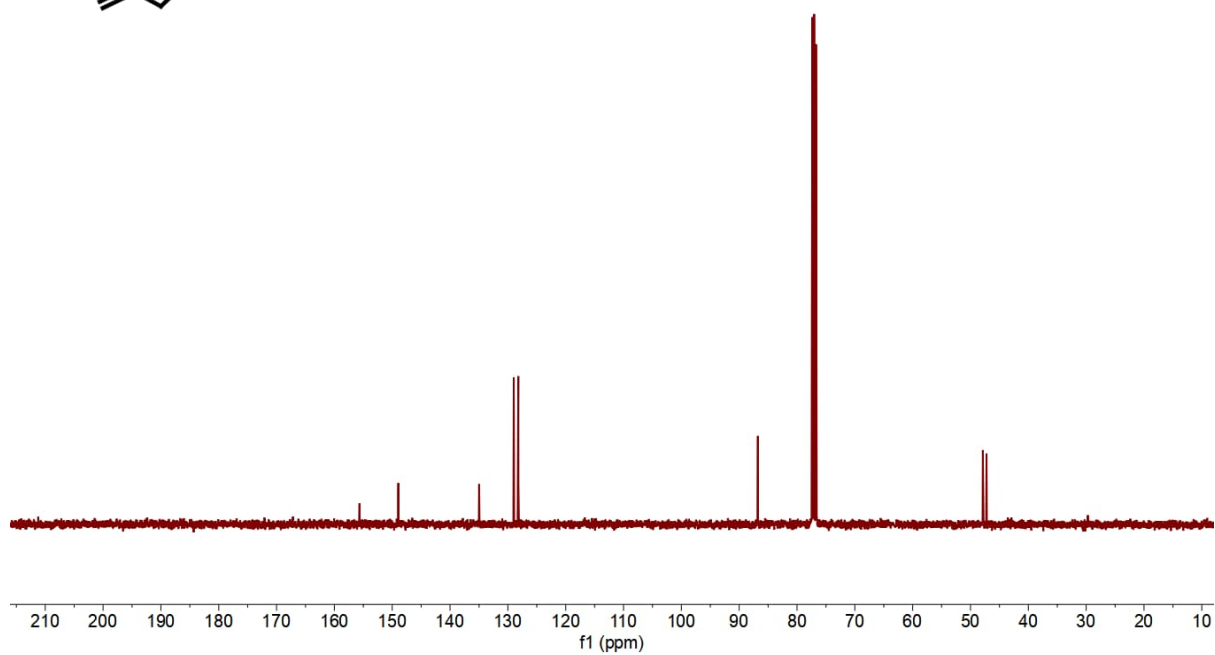
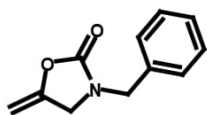


¹³C NMR spectrum of 2a

2b

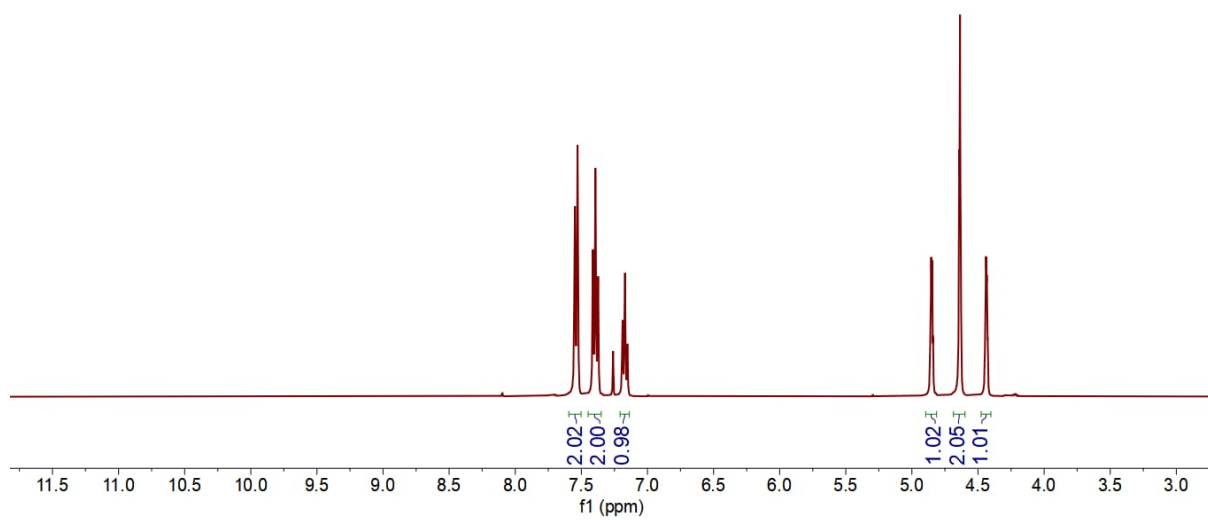
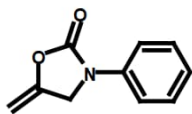


¹H NMR spectrum of 2b

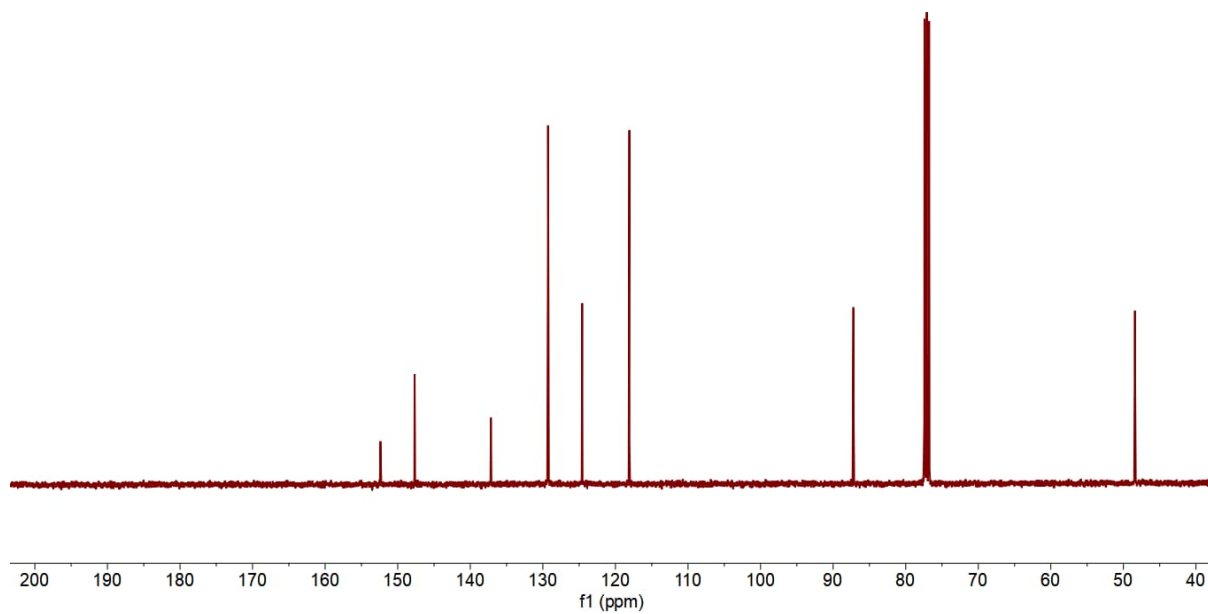
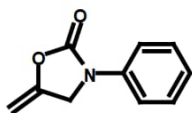


¹³C NMR spectrum of 2b

2c

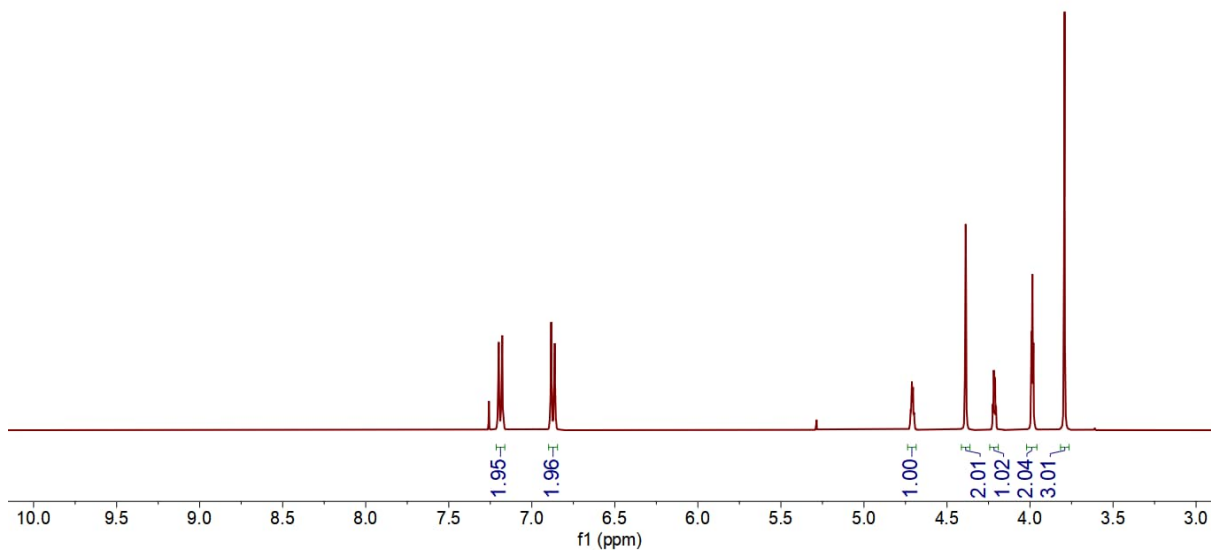
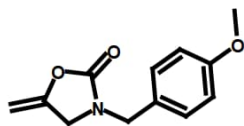


¹H NMR spectrum of 2c

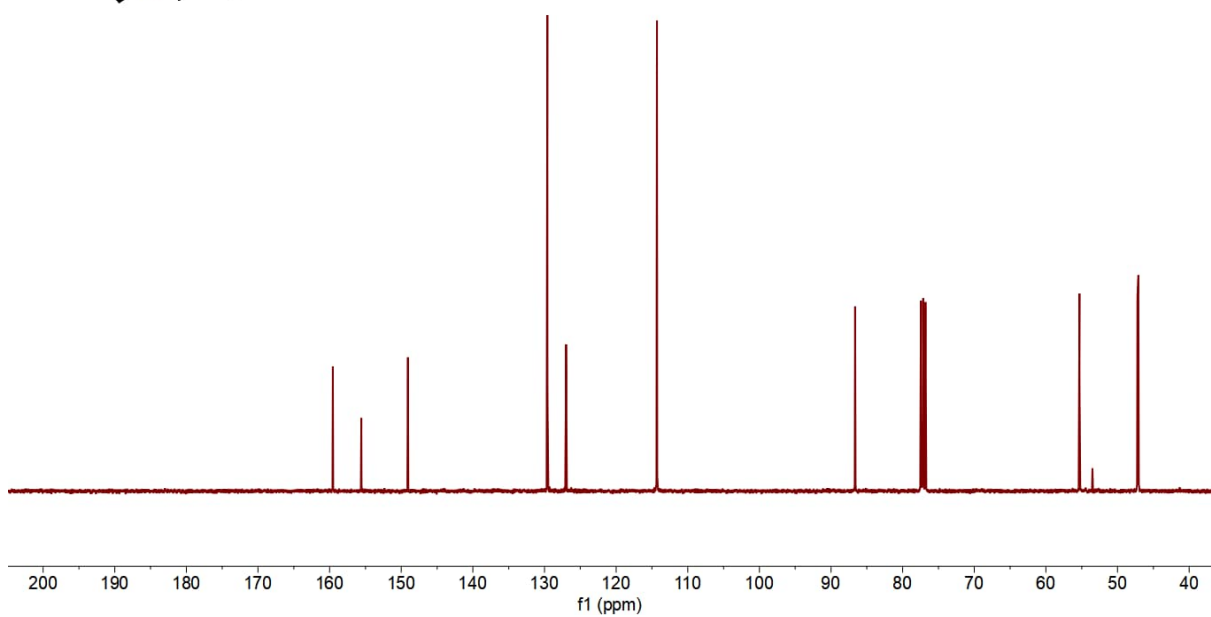
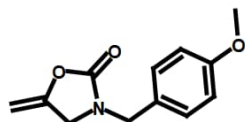


¹³C NMR spectrum of 2c

2d

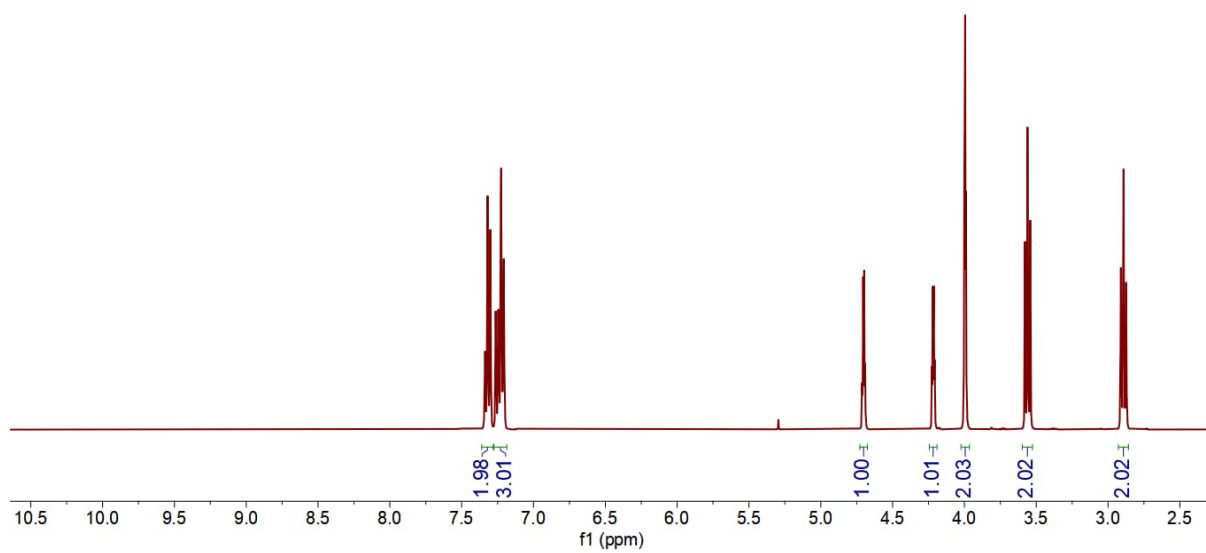
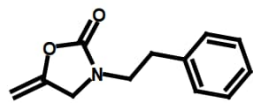


¹H NMR spectrum of 2d

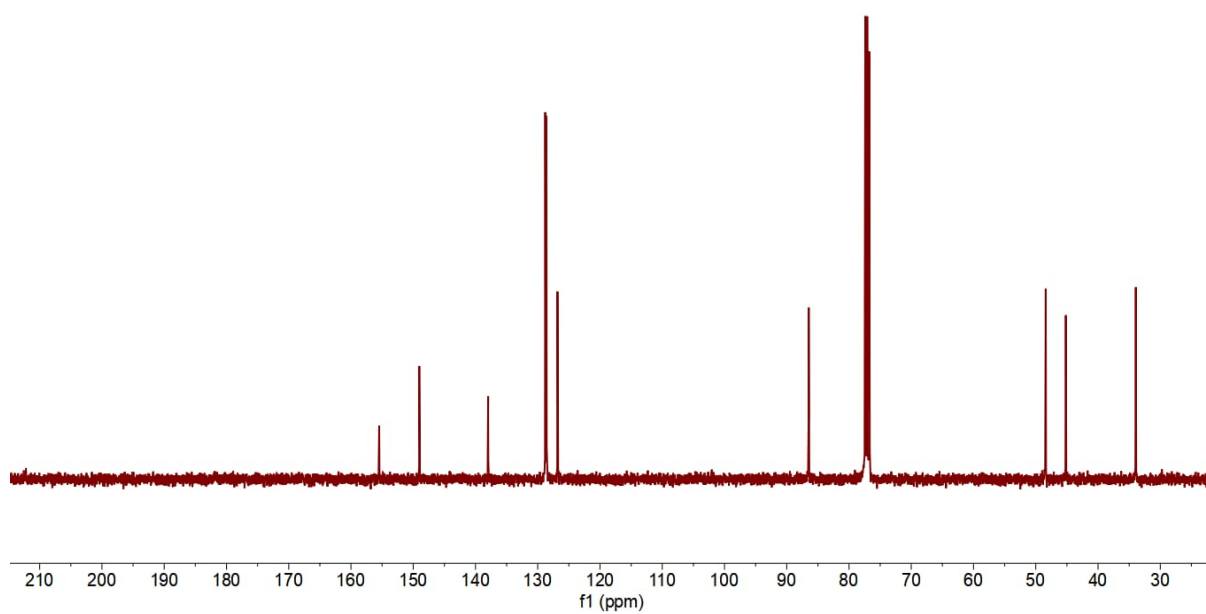
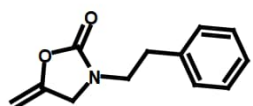


¹³C NMR spectrum of 2d

2e



¹H NMR spectrum of 2e



¹³C NMR spectrum of 2e

References:

1. Y.-L. Shen, J.-L. Jin, G.-X. Duan, P.-Y. Yu, Y.-P. Xie, X. Lu, *Chem. Eur. J.*, 2021, 27, 1122
2. B. K. Teo, Y. H. Xu, B. Y. Zhong, Y. K. He, H. Y. Chen, W. Qian, Y. J. Deng, Y. H. Zou, *Inorg. Chem.*, 2001, 40, 6794–6801
3. S. Hug, L. Stegbauer, H. Oh, M. Hirscher, B. V. Lotsch, *Chem. Mater.*, 2015, 27, 8001-8010.
4. J. Chen, L. Jiang, W. Wang, Z. Shen, S. Liu, X. Li, Y. Wang, *J. Colloid Interface Sci.*, 2022, 609, 775-84
5. H. Kuan, F. Liu, S. Dai. *J. Mater. Chem. A.*, 2016, 4, 13063-13070
6. Y. Zhao, K.-X. Yao, B. Teng, T. Zhang, Y. Han, *Energy Environ. Sci.*, 2013, 6, 3684-3692
7. K.-A. Fayemiwo, G.-T. Vladislavljević, S.-A. Nabavi, B. Benyahia, D.-P. Hanak, K.-N. Loponov, V. Manovic, *Chem. Eng. J.*, 2018, 334, 2004-2013
8. Y. Li, L. Yang, X. Zhu, J. Hu, H. Liu, *Int. J. Coal Sci. Technol.*, 2017, 4, 50-59
9. J.-F. Guo, L.-Z. Wang, D. Zhang, J.-H. Huang, *Energy Fuels*, 2020, 34, 9771-9778.
10. J. Yan, B. Zhang, Z. Wang, *Polym. Chem.*, 2016, 7, 7295-7303
11. G. Wang, K. Leus, H.-S. Jena, C. Krishnaraj, S. Zhao, H. Depauw, N. Tahir, Y.-Y. Liu, P. Van Der Voort, *J. Mater. Chem. A*, 2018, 6, 6370-6375
12. Z. Yang, S. Wang, Z. Zhang, W. Guo, K. Jie, M.-I. Hashim, O.-Š. Miljanić, D.-E. Jiang, I. Popovs, S. Dai, *J. Mater. Chem. A*, 2019, 7, 17277-17282
13. A. Pedrini, J. Perego, S. Bracco, C.-X. Bezuidenhout, P. Sozzani, A. Comotti, *J. Mater. Chem. A*, 2021, 9, 27353-27360
14. A. Hassan, S. Goswami, A. Alam, R. Bera, N. Das, *Sep. Purif. Technol.*, 2021, 257, 117923
15. A.-L. Gu, W.-T. Wang, X.-Y. Cheng, T.-D. Hu, Z.-L. Wu, *Inorg. Chem.*, 2021, 60, 13425–13433
16. L. Li, Y. Lv, H. Sheng, Y. Du, H. Li, Y. Yun, Z. Zhang, H. Yu, M. Zhu, *Nat. Commun.*, 2023, 14, 6989.
17. Y. Liu, X. Chai, X. Cai, M. Chen, R. Jin, W. Ding, Y. Zhu, *Angew. Chem. Int. Ed.*, 2018, 57, 9775-9779.
18. M. Zhao, S. Huang, Q. Fu, W. Li, R. Guo, Q. Yao, F. Wang, P. Cui, C. H. Tung, D. Sun, *Angew. Chem. Int. Ed.*, 2020, 59, 20031-20036
19. Q. Cao, L. L. Zhang, C. Zhou, J. H. He, A. Marcomini, J. M. Lu, *Appl. Catal. B*, 2021, 294, 120238
20. X. Yu, Z. Yang, F. Zhang, Z. Liu, P. Yang, H. Zhang, B. Yu, Y. Zhao, Z. Liu, *Chem. Commun.*, 2019, 55, 12475-12478
21. S. Ghosh, S. Riyajuddin, S. Sarkar, K. Ghosh, S. M. Islam *ChemNanoMat*, 2020, 6, 160-172